

LA-8186-MS

Informal Report

C.3

CIC-14 REPORT COLLECTION

**REPRODUCTION
COPY**

**The Dense Z-Pinch (DZP) as a Fusion Power Reactor:
Preliminary Scaling Calculations
and Systems Energy Balance**

University of California



LOS ALAMOS SCIENTIFIC LABORATORY

Post Office Box 1663 Los Alamos, New Mexico 87545

An Affirmative Action/Equal Opportunity Employer

This report was not edited by the Technical Information staff.

This work was supported by the US Department of Energy, Office of Fusion Energy.

This report was prepared as an account of work sponsored by the United States Government. Neither the United States nor the United States Department of Energy, nor any of their employees, nor any of their contractors, subcontractors, or their employees, makes any warranty, express or implied, or assumes any legal liability or responsibility for the accuracy, completeness, or usefulness of any information, apparatus, product, or process disclosed, or represents that its use would not infringe privately owned rights.

**UNITED STATES
DEPARTMENT OF ENERGY
CONTRACT W-7408-ENG. 36**

LA-8186-MS
Informal Report
UC-20d
Issued: January 1980

**The Dense Z-Pinch (DZP) as a Fusion Power Reactor:
Preliminary Scaling Calculations
and Systems Energy Balance**

R. L. Hagenson
A. S. Tai*
R. A. Krakowski
R. W. Moses



* Laboratoire de Genie Atomique, Ecole Polytechnique
Federal de Lausanne, Switzerland.



CONTENTS

ABSTRACT	1
I. EXECUTIVE SUMMARY	2
II. INTRODUCTION	3
III. ANALYTIC PLASMA AND REACTOR MODEL	6
A. Spatially-Averaged Point Plasma Model	6
B. Plasma Energy Balance	8
C. Evaluation of Plasma Model	10
D. Formulation of Plasma Performance Criterion	13
E. Physics Constraints and Preliminary Design-Point Evaluation	16
1. Particle Drifts	16
2. Alpha-Particle Containment	19
3. Fuel Burnup/Depletion	20
4. Energy Replacement	22
5. Preliminary Physics Operating Point Based Upon Analytic Model	22
IV. DETERMINATION OF PHYSICS OPERATING POINT	24
A. Engineering Energy Balance	24
B. Description of Numerical Point Model	26
C. Parameter Study	27
D. Physics Design Point	29
V. PRELIMINARY ENGINEERING CONSIDERATIONS	32
A. Voltage and Power Supply Requirements	32
B. Reactor Configuration	35
VI. SUMMARY CONCLUSIONS and RECOMMENDATIONS	35
REFERENCES	39
APPENDICES	
A. Description of DZP Experiment and Comparison of Plasma Model with Experimental Results	41
B. Description of DZP/MHS Code and Comparison with Zero-Dimensional Results	44
1. DENSZP Plasma Model	44
a. General Operation	44
b. Radial Transport	45
2. Results and Comparisons	46

THE DENSE Z-PINCH (DZP) AS A FUSION POWER REACTOR:
PRELIMINARY SCALING CALCULATIONS AND SYSTEMS ENERGY BALANCE

R. L. Hagenson, A. S. Tai, R. A. Krakowski, and R. W. Moses

ABSTRACT

A conceptual DT fusion reactor concept is described that is based upon the dense Z-pinch (DZP). This study emphasizes plasma modeling and the parametric assessment of the reactor energy balance. To this end simple analytic and numerical models have been developed and evaluated. The resulting optimal reactor operating point promises a high-Q, low-yield system of a scale that may allow the use of conventional high-voltage Marx/water-line technology to drive a potentially very small reactor system.

I. EXECUTIVE SUMMARY

As part of an overall assessment of the reactor potential of a number of alternative magnetic fusion concepts, the Office of Fusion Energy, US Department of Energy, has funded systems studies according to a three tier structure. These studies are categorized in order of decreasing level of effort and detail as Level I, Level II, and Level III. The highest level of study (Level I) would include in a multi-man-year effort considerable conceptual design and economic analysis, in addition to sophisticated, state-of-the-art physics and operating-point analyses. The lowest level of study (Level III) would characterize less understood and developed confinement schemes by means of relatively simple physics models and parametric analysis of potential reactor operating points. Generally, a Level III study would not provide a reactor embodiment per se, and, because of obvious gaps in the physics understanding of these relatively unexplored concepts, only a range of potential reactor operating points may be parametrically identified. The Dense Z-Pinch Reactor (DZPR) study described herein is a Level III study.

The DZPR concept and the related system energy balance is eloquently simple; a high electrical current is initiated along a sub-millimeter current channel within a high-pressure DT gas, and the ohmically-heated filament of DT plasma would produce a thermonuclear yield that is ~ 20 - 40 times as great as the energy delivered to the pinch as magnetic field and ohmic dissipation. Both the analytic and numerical scaling that has been developed and evaluated in subsequent sections of this report indicate a well-defined optimum operating point for the DZPR. This optimum embodies a ~ 0.1 -mm-radius by 0.1 -m-long pinch that requires ~ 140 kJ of energy to be delivered in ~ 300 ns, resulting in a 4.4 -MJ and $Q \sim 30$ thermonuclear yield. For typical reactor parameters, this operating point yields an engineering Q -value \bar{Q} equal to 7.9 (recirculating power fraction of 0.13). The ~ 2 - μ s burn estimate does not account for gas ingestion by the plasma column, specifies that no alpha-particle heating occurs, and neglects coronal and diffusive processes. Furthermore, the DZP plasma column has been assumed to be MHD stable throughout the burn period. The majority of plasma heating is provided by ohmic dissipation; shock processes should not occur, are ignored and are considered undesirable; compressional heating is negligible for the optimal mode of DZPR operation. Table I summarizes the DZPR physics design point that has emerged from this study.

TABLE I
TYPICAL DZPR DESIGN PARAMETERS

<u>Parameter</u>	<u>Value</u>
Initial plasma radius (mm)	0.1
Plasma length (m) ^(a)	0.1
Plasma density ($10^{27}/\text{m}^3$) ^(b)	1.08
Plasma line density ($10^{19}/\text{m}$)	3.40
Peak plasma current (MA)	1.45
Plasma current risetime (μs)	0.31
Burn time (μs) ^(c)	2.0
Input (Marx-bank) energy (kJ)	140
Fusion yield (MJ) ^(d)	4.4
Plasma Q-value ^(e)	33.3
Lawson parameter ($10^{21}\text{s}/\text{m}^3$)	9.75

(a) arbitrarily selected

(b) corresponds to an initial DT filling pressure of $1.5(10)^4$ Torr (20.3 atm)

(c) A 10-keV temperature is achieved in $0.3\mu\text{s}$

(d) Based on 14.1-MeV neutrons with a blanket multiplication of 1.17 and 3.5-MeV alpha particles. The alpha-particle energy is assumed not to contribute to the plasma heating

(e) Ratio of fusion yield to input Marx-bank energy, which is computed by means of a detailed circuit code to be delivered to the pinch with 95% efficiency, assuming a realistic switching sequence.

The primary emphasis of this study has been the modeling of plasma yield and energy balance for the DZP concept. No attempt has been made to elucidate the reactor embodiment in terms of the mechanical, thermohydraulic, and neutronic layout. The low thermonuclear yield derived from each discharge will, however, require either a multichannel discharge and/or a high repetition-rate operation if total powers in the 100's Mwt range are desired. Furthermore, the design of the low-energy, high-voltage Marx/water-line energy source needed to drive the high-repetition-rate DZPR will place definite constraints on any future attempts to generate a physical reactor layout; quantification of this crucial design constraint, however, could not be completed within the scope of this study.

II. INTRODUCTION

In the simplest form, a Z-pinch can be represented by a cylindrical plasma column through which an axial electric current is passed to produce a rapidly increasing and constricting magnetic field. One of the major problems associated with the simple pinch devices has been that of MHD instability.

The simple Z-pinch and its sausage and kink instabilities have been observed and studied since the beginning of thermonuclear fusion research.¹⁻³ The instability growth occurred in a period equal approximately to the transit time of sound across the pinched column. Recent MHD stability analyses, however, have indicated that greater stability may be expected for pinches that are diffuse⁴⁻⁶ or embedded in dense gas;⁷ finite-Larmor-radius effects,^{8,9} or plasma flow,¹⁰ may also lead to greater stability. Since the Z-pinch has the potential of producing very high constricting magnetic fields, the plasma density could be sufficiently increased to satisfy the Lawson criterion in a relatively short confinement or burn time. In an early experiment thermonuclear plasmas with a density equal to $\sim 10^{25} \text{ m}^{-3}$ and a Lawson parameter close to 10^{19} s/m^3 have been reported.¹¹ More recent experiments used an electron-beam trigger¹² to initiate a DZP, but this approach was characterized by low voltage and a long dwell-time. Recently, one and two-dimensional numerical calculations of a Z-pinch plasma, that would be compressed by means of a solid liner moving at velocities of $\sim 10^4 \text{ m/s}$, have indicated that thermonuclear temperatures of nearly 20 keV could be achieved.¹³

The simple configuration of the Z-pinch and the possibility of realizing a high plasma density make the dense Z-pinch (DZP) an attractive alternate approach to fusion power in terms of power density, power level, and physical size. If a small and dense Z-pinch could be stabilized for times sufficiently long to realize a high energy gain (i.e., a few microseconds), the associated reactor system would offer advantages of simplicity and low power output, leading to a potentially economic and highly modular power system. A conceptual DZP reactor has been proposed.¹⁴ The plasmas for the design given in Ref. 14 is small (2.2-mm diameter and 100-mm long) and dense ($3.2(10)^{26} \text{ m}^{-3}$). A final temperature of 41 keV, a short burning time ($\sim 2.5 \mu\text{s}$) and a low output power (100 MWe) was proposed. The reactor analysis given in Ref. 14, however, modeled the plasma response only during the initiation/start-up phase, using an unclear extrapolation method to estimate the final plasma yields and Q-values. Because of the ambiguity injected by using such extrapolations, the order of magnitude difference between thermonuclear yields required to give Q-values that are comparable to the results presented herein could not be resolved; the present study

indicates desirable reactor Q-values can be achieved for yields in the ~ 5-MJ range, rather than the ~ 55-MJ range indicated in Ref. 14.

The present study first reassesses the simple analytic model of a stationary Z-pinch proposed by Hammel.¹⁵ This model considers an ohmically-heating DZP operating with a constant radius, and optimistically eliminates radial shocks and transport. Nevertheless, such a model is valuable in regard to its simple analytic nature, its role in testing more realistic burn codes and the possibility for serving as an idealized reference case for examining reactor performance. In addition to a comparison of the results given by this simple analytic model with those given by more detailed burn codes, implications of a constant-radius operation upon a DZP reactor are examined from the viewpoint of system energy balance.

The predictions of this idealized analytic plasma model, however, are based upon the assumption of constant radius operation. The ability to operate within this highly specialized current limit depends crucially upon the electrical characteristics of the driving circuit as well as fundamental physical processes occurring within the pinch and surrounding corona. Consequently, a realistic model of a Marx-bank/water-line power supply has been coupled to a three-particle (alpha particles, electrons, and ions) zero-dimensional burn code, and the zero-dimensional burn model has been evaluated to yield the final, but preliminary, estimate of a DZPR physics operating point. The availability of the analytical model, however, has proven useful in guiding these numerical studies. The technological implications of the required electrical circuit, which does not necessarily lead to operation precisely at the constant-radius current limit, additionally can be addressed. Modeling of cold gas/plasma ingestion and recycling from the dense gas/corona region surrounding the DZP, however, proved to be beyond the scope of this study, although detail analysis of these complex processes is in progress.¹⁶ Experimental work is also being conducted¹⁷ to study the ohmically-heated, gas-embedded DZP; the status of this experiment is summarized in Appendix A.

Generally, the predictions of this Level III conceptual physics design study are encouraging and promising. These results should be used to guide a more detailed physics and technology assessment of the DZPR, particularly when further positive progress is made on both experimental¹⁷ and theoretical¹⁶ fronts. It is concluded that, within the limits of the clearly stated

assumptions upon which this Level III study is based, the DZP represents an attractive approach to small-sized, uncomplicated fusion power.

III. ANALYTIC PLASMA and REACTOR MODEL

A. Spatially Averaged Point Plasma Model

The time-dependent, point model of a gas-embedded DZP is depicted in Fig. 1. This model is based upon the following assumptions:

- MHD stability of the cylindrical plasma column for all computations.
- Transport coefficients (ion thermal conductivity, electrical resistivity) are given by classical theories.
- Equal temperature for electrons and ions.
- Pressure balance exists at all plasma radii, and radially averaged plasma parameters are used by the analytic point model.
- Only a stationary (constant radius and plasma density) pinch is considered.
- Neither the electric circuit driving the pinch current, nor corona and/or shock formation in the dense gas or peripheral diffuse plasma are taken into account.

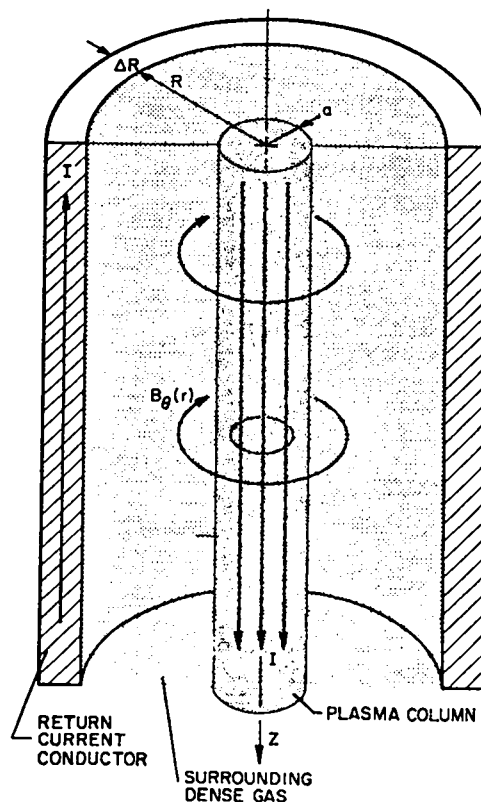


Fig. 1.

Schematic representation of a gas-embedded dense Z-pinch (DZP) used to formulate the analytic reactor model.

- The current density is assumed to be uniform in the pinch and to follow a time trajectory that assures a constant pinch radius. This assumption implies a continual adjustment of the external circuitry.

A number of these assumptions are examined in Sec. IV by a time-dependent computer model that has been developed to resolve the interaction between a zero-dimensional (point) plasma with a realistically simulated circuit. Nevertheless, the analytic model developed and evaluated in this section offers the advantages of simplicity while simultaneously giving a relatively accurate description of the DZP behavior.

The pressure balance across the pinch (Fig. 1) at radius $r < a$ for a uniform current density is expressed by

$$2nk_B T + B_\theta^2/2\mu_0 = (2/r^2) \int_0^r 2nk_B T r dr \quad , \quad (1)$$

where $B_\theta(r) = B_{\theta 0} r/a$ is the poloidal magnetic field, n is the local plasma density, and a is the plasma radius. Implicit in Eq. (1) is the assumption that inertial terms can be neglected; the sound transit time is small compared to the burn time, and shocks will not form. MKS units are consistently used, except for the temperature $T(\text{keV})$; k_B is the Boltzmann constant ($1.602(10)^{-16}$ J/keV) and $\mu_0 = 4\pi(10)^{-7}$ H/m. If the plasma temperature is assumed uniform across the pinch radius, as has been shown by numerical computations (Appendix B) using classical ion cross-field thermal conductivity and uniform current density, Eq. (1) can be differentiated to yield

$$dn/dr + (2n_0/\langle\beta\rangle)(r/a^2) = 0 \quad , \quad (2)$$

where $\langle\beta\rangle \equiv (n_0 k_B T)/(B_{\theta 0}^2/2\mu_0)$, $n_0 \equiv n(r=0)$ is the central plasma density and $B_{\theta 0}$ is the magnetic field at the plasma edge.

Integration of Eq. (2) gives

$$n(r) = n_0 [1 - (r/a)^2/\langle\beta\rangle] \quad . \quad (3)$$

In order to assure that the plasma density at $r = a$ is zero, $\langle \beta \rangle$ must be equal to 1. Consequently, the density profile must be parabolic for this constant pressure approximation. Hence,

$$n(r) = n_0 [1 - (r/a)^2] \quad , \quad (4)$$

and the volume-averaged plasma parameters are given by $\langle n \rangle = n_0/2$, $\langle n^2 \rangle = n_0^2/3$, $\langle B_\theta \rangle = 2B_{\theta 0}/3$ and $\langle B_\theta^2 \rangle = B_{\theta 0}^2/2$. Consequently, $\langle \beta \rangle$ represents the ratio of the mean plasma pressure to the mean magnetic pressure, and $\langle \beta \rangle = 1$ leads to

$$n_0 k_B T = B_{\theta 0}^2 / 2\mu_0 \quad . \quad (5)$$

In addition, the line density, $N(\text{m}^{-1})$, is given by

$$N = \pi a^2 \langle n \rangle = \pi a^2 n_0 / 2 \quad . \quad (6)$$

B. Plasma Energy Balance

The volume-averaged plasma energy balance used for the time-dependent point model (Sec. IV) is given by

$$\frac{d}{dt} \left(\frac{3}{2} n_0 k_B T \right) \equiv f_\alpha P_\alpha + P_{\text{OHM}} - P_{\text{BR}} - P_{\text{COND}} - n_0 k_B T (d \ln a^2 / dt) \quad . \quad (7)$$

where the last term is zero for the constant radius case considered by this analytic formulation.

The alpha-particle power density, P_α , a fraction f_α of which may contribute to the plasma heating, is given by

$$P_\alpha (\text{W/m}^3) \approx \frac{1}{4} \langle n^2 \rangle \langle \sigma v \rangle E_\alpha \quad , \quad (8)$$

where $\langle \sigma v \rangle$ is the velocity-averaged DT cross section, and E_α is the alpha-particle energy. P_{OHM} is the ohmic-heating power density and is approximated by the following expression for the case of uniform current

$$P_{\text{OHM}}(\text{W/m}^3) = \eta_{\perp} [I / (\pi a^2)]^2, \quad (9)$$

where η_{\perp} is the electrical resistivity perpendicular to the magnetic field, and I is the total plasma current. The bremsstrahlung power loss is given by

$$P_{\text{BR}}(\text{W/m}^3) = 5.35(10)^{-37} \langle n^2 \rangle Z_{\text{eff}} T^{1/2}, \quad (10)$$

where Z_{eff} is the effective charge number. The energy loss associated with radial thermal conduction is approximated by

$$P_{\text{COND}}(\text{W/m}^3) \approx 2f_{\text{COND}} k_{\perp} T / a^2. \quad (11)$$

The conduction term, P_{COND} , represents an ad hoc addition made to examine the influence of an effective radial loss, where f_{COND} is an arbitrary parameter; the radial transport problem is complex, and the form assumed for P_{COND} that uses a thermal gradient equal to $\sim T/a$ should be considered only as a rough measure of radial conduction losses to a zero-temperature sink. This aspect of the DZP model requires a level of analysis that is beyond the scope of this study. Axial losses from the pinch column are generally ignored, although this issue is addressed in Sec. III.E.

For the cross-field electric resistivity, η_{\perp} , and the ion cross-field thermal conductivity, k_{\perp} , the following expressions are used^{18, 19}

$$\eta_{\perp}(\Omega \text{ m}) = \eta_{\parallel} / 0.51 \quad (12)$$

$$k_{\perp}(\text{W/m keV}) = \zeta \langle n^2 \rangle / (\langle B_{\theta}^2 \rangle T^{1/2}), \quad (13)$$

where

$$\begin{aligned} \eta_{\parallel} &= 9.62(10)^{-10} Z_{\text{eff}} \ln \Lambda / (\gamma_E T^{3/2}) \\ \gamma_E &= 0.582 + 0.418 [(Z_{\text{eff}} - 1) / Z_{\text{eff}}]^2 \\ \Lambda &= 9.34(10)^{16} T / (Z_{\text{eff}} \langle n \rangle^{1/2}) \\ \zeta &= 5.07(10)^{-39} A_i^{1/2} \ln \Lambda \quad , \end{aligned} \tag{14}$$

Again, except for the temperature, $T(\text{keV})$, mks units are used in Eqs. (12-14), and A_i is taken as 2.5 for D-T.

C. Evaluation of Plasma Model

For the case where heating by alpha particles and thermal losses by radial thermal conduction can be ignored ($f_{\alpha} \approx f_{\text{COND}} \approx 0$), Eq. (7) predicts an equilibrium plasma temperature, T_{EQ} , given by the condition $dT/dt = 0$. When volume averages are taken into account, the following expression gives T_{EQ}

$$T_{\text{EQ}}(\text{keV}) = 9.25(10)^{18} \ln \Lambda / (\langle n \rangle a^2) = 2.91(10)^{19} \ln \Lambda / N \quad . \tag{15}$$

Defining an effective time constant and temporal normalization,

$$\tau(\text{s}) \equiv 6.73(10)^{20} T_{\text{EQ}}^{1/2} / \langle n \rangle = 3.63(10)^{30} (\ln \Lambda)^{1/2} / (\langle n \rangle N^{1/2}) \quad , \tag{16}$$

with $\theta \equiv T/T_{\text{EQ}}$, $\xi \equiv t/\tau$, and taking Eqs. (9)-(14) into account while neglecting the alpha-particle heating (i.e., $f_{\alpha} P_{\alpha} \ll P_{\text{OHM}}$), Eq. (7) can be written as follows

$$d\theta/d\xi = (1 - 6.79 f_{\text{COND}}) / \theta^{1/2} - \theta^{1/2} \tag{17}$$

Since the total plasma current, I , is given by $I = 2\pi a B_{\theta 0} / \mu_0$ it follows by means of Eq. (9) that

$$I^2(A^2) = 6.41 \times (10)^{-9} NT \quad . \quad (18)$$

Hence, using Eq. (14), the current, I_{EQ} , corresponding to T_{EQ} is given by

$$I_{EQ}(A) = 4.31(10)^5 (\ln \Lambda)^{1/2} \quad , \quad (19)$$

and $I/I_{EQ} = \theta^{1/2}$; $I_{EQ} = 1.36$ MA for $\ln \Lambda = 10$. This current limit is a constant for all pinches²⁰ and is called the "Pease current". The pinch will either expand radially if the current is smaller than I_{EQ} , or the pinch will collapse if I exceeds I_{EQ} .

Equation (17) shows that a steady-state solution exists only for a condition where radial conduction losses do not exceed the value corresponding to $f_{COND} = 0.147$, as predicted by the approximate and classical formulation. The solution of Eq. (17) is given by

$$\xi = \frac{1}{\theta_{EQ}^{1/2}} \ln \frac{\theta_{EQ}^{1/2} + \theta^{1/2}}{\theta_{EQ}^{1/2} - \theta^{1/2}} - 2\theta^{1/2} \quad , \quad (20)$$

with $0 < \theta < \theta_{EQ} < 1$, where

$$\theta_{EQ} \equiv 1 - 6.79 f_{COND} \quad . \quad (21)$$

Equation (20) is plotted in Fig. 2 for a range of f_{COND} values. Generally, the effect of thermal conduction losses reduces the final equilibrium temperature by a factor θ_{EQ} . Shown also for comparison in Fig. 2 is a simple exponential function; it appears that the time constant or scaling parameter, τ (Eq. 16), can be regarded as an effective rise time for the

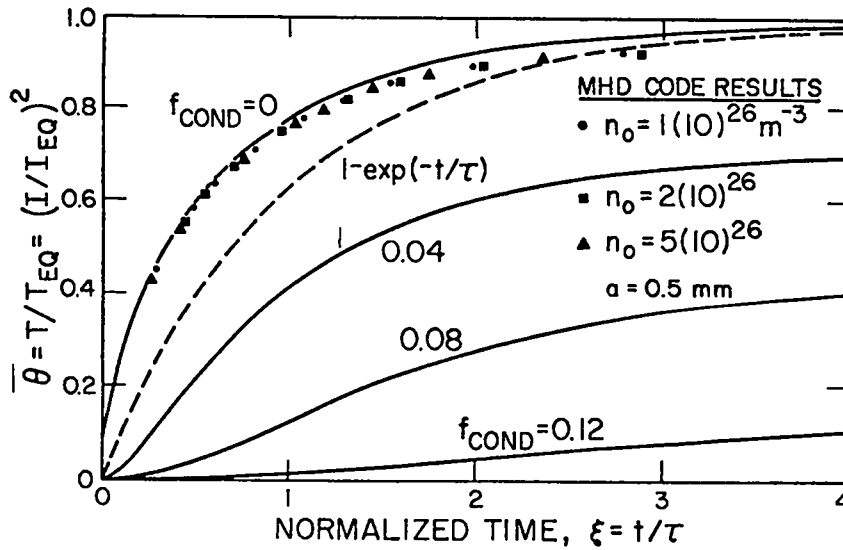


Fig. 2.

Comparison of the solution to Eq. (17) for a range of radial conduction parameters with the results of a radial MHS burn code computation.

plasma temperature ($T = 0.777T_{EQ}$ at $t = \tau$ when $f_{COND} = 0$) and the associated current needed to fulfill the Pease requirement, I_{EQ} . Equation (20) is also compared in Fig. 2 with the results given by a radial magnetohydrostatic (MHS) burn code (Appendix B); the deviation between the analytic and computer models is within a few percent for a range of plasma densities of interest.

The following expression for a Lawson-like parameter can be obtained from Eq. (16)

$$\langle n \rangle \tau (\text{s/m}^3) = 6.73(10)^{20} T_{EQ}^{1/2} = 3.63(10)^{30} (\ln \Lambda)^{1/2} / N^{1/2} \quad . \quad (22)$$

Figure 3 shows the dependence of T_{EQ} and $\langle n \rangle \tau$ on the plasma line density, N , for $\ln \Lambda = 10$. The performance of the DZP, as measured by $\langle n \rangle \tau$, where τ is given by Eq. (16), depends only on the line density. As is shown in Sec. IV.C., however, the system performance of a DZPR, as measured by a plasma Q-value, shows a very sharp optimum in line density.

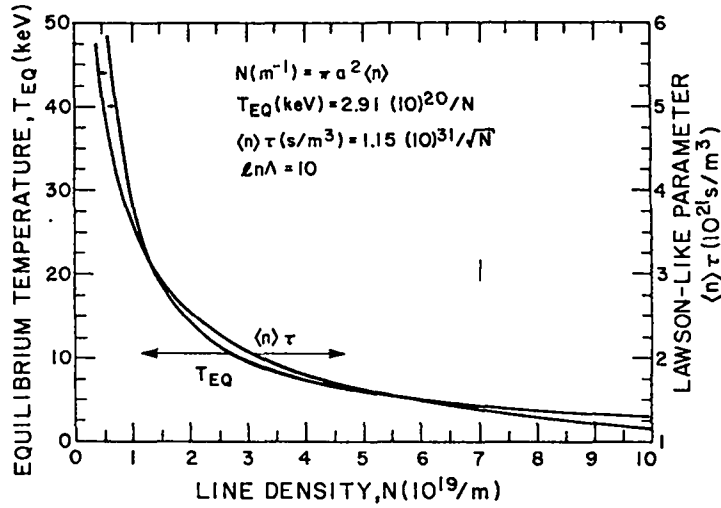


Fig. 3.

Graphical display of Eqs. (15) and (22) showing the dependence of T_{EQ} and $\langle n \rangle \tau$ on line density, N .

D. Formulation of Plasma Performance Criterion

Before an estimate of important DZPR characteristics can be made, a performance criterion or Q -value must be formulated. First, given a radius R for the return conductor (Fig. 1), the magnetic field energy contained in the cylinder per unit pinch length is given by

$$W_B(\text{J/m}) = \mu_0 I_{EQ}^2 \theta [\ln(R/a) + 1/4] / 4\pi \quad . \quad (23)$$

Since I_{EQ} is essentially a constant, as given by Eq. (19) for this constant-radius case, W_B depends only on θ or on $\xi = t/\tau$ for a given value of R/a . The time symbol " t " previously used for time will be replaced at this point by the burn time, τ_B , to represent the duration of the thermonuclear reactions.

Under the approximation that $\langle \sigma v \rangle / T^2$ equals a constant in the temperature range of interest, the thermonuclear yield per unit pinch length can be written

$$W_T(\text{J/m}) = (\pi a^2 E_F / 4) \langle \sigma v \rangle_{EQ} \langle n^2 \rangle \tau \theta g(\theta) \quad , \quad (24)$$

where E_F is the fusion energy yield (alpha particles and neutrons), $\langle\sigma v\rangle_{EQ}$ is the value of $\langle\sigma v\rangle$ at T_{EQ} , and

$$g(\theta) \equiv \frac{1}{\theta} \int_0^\xi \theta^2 d\xi \quad . \quad (25)$$

Using Eq. (17), integration of Eq. (25) gives

$$g(\theta) = \frac{\theta_{EQ}^{5/4}}{\theta} \ln \frac{\theta_{EQ}^{1/4} + \theta^{1/2}}{\theta_{EQ}^{1/4} - \theta^{1/2}} - 2(\theta^{2/3}/5 + \theta_{EQ}^{1/2}\theta^{1/2}/3 + \theta_{EQ}/\theta^{1/2}), \quad (26)$$

where, again, θ_{EQ} is given by Eq. (21). The function $g(\theta)$ decreases rapidly with decreasing values of θ_{EQ} (i.e., with increasing f_{COND}). For the case when $\theta_{EQ} = 1$ (i.e., $f_{COND} = 0$), $g(\theta) \approx \xi - 1$ as θ approaches unity (i.e.,

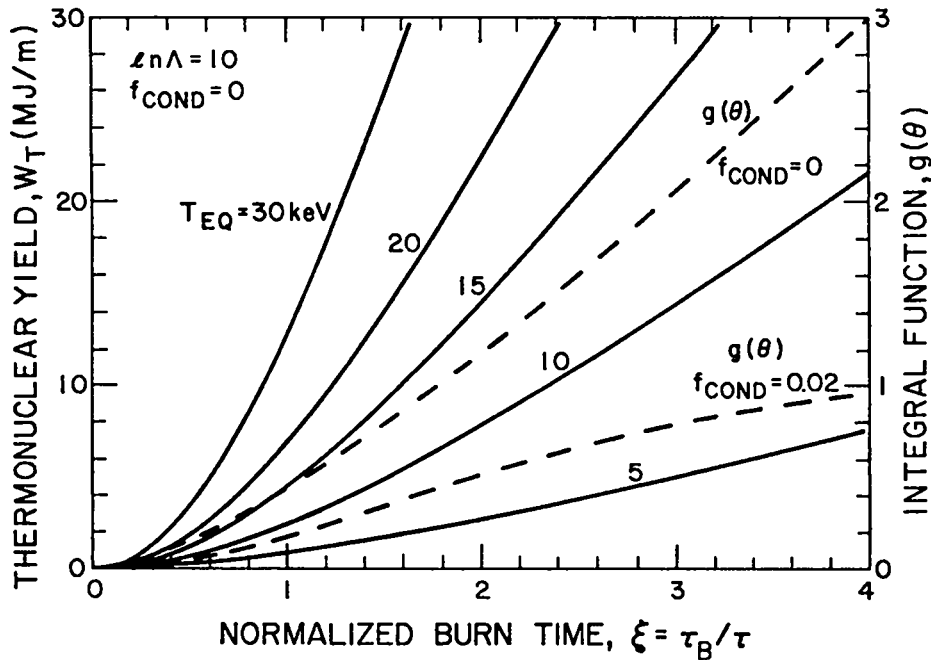


Fig. 4.

Dependence of thermonuclear yield, W_T (Eq. (24)), and the function $g(\theta)$ (Eq. (26)) on $\xi = \tau_B/\tau$, where τ is given by Eq. (16).

$\xi > 3$), as can be seen from Eqs. (20) and (26). This behavior is shown in Fig. 4 (dashed lines). The plasma Q-value is defined as

$$Q \equiv W_T/W_{IN} \quad , \quad (27)$$

where W_{IN} is the total input energy delivered to the pinch. In the present case W_B is equal to the stored field energy, as given by Eq. (23). Taking $E_F = 3.2(10)^{-12}$ J (i.e., 20 MeV/n), assuming a blanket multiplication of 1.17 and $\langle \sigma v \rangle_{EQ}/T_{EQ}^2 = 1.1(10)^{-24}$ m³/s keV² (within 10% in the temperature range of interest), W_T and Q become

$$W_T(\text{J/m}) = 2.29(10)^4 \ln \Lambda T_{EQ}^{3/2} \theta g(\theta) \quad (28)$$

$$Q = 1.23 T_{EQ}^{2/3} g(\theta) / [\ln(R/a) + 0.25] \quad (29)$$

Since $\theta \approx 1$ for $\tau_B/\tau \gtrsim 3$, Q is proportional to W_T , which is proportional to $T_{EQ}^{3/2} g(\theta)$ for a given radius ratio R/a. Additionally, if $f_{COND} = 0$, (i.e., $g(\theta) \approx \tau_B/\tau - 1$), it follows that

$$Q \propto W_T \propto T_{EQ}^{3/2} (\tau_B/\tau - 1) \quad . \quad (30)$$

For $\tau_B \gg \tau$ and taking Eqs. (15) and (16) into account, Eq. (30) becomes

$$Q \propto W_T \propto \tau_B T_{EQ} \propto \tau_B / \langle n \rangle a^2 \quad (31)$$

Therefore, smaller plasma radii or plasma line densities predicted to lead to higher plasma Q-values. As noted previously, however, the more detailed calculations in Sec. IV.B actually predict a well-defined optimum N.

Taking $\ln \Lambda = 10$, the dependence of W_T on ξ for the case where $f_{COND} = 0$ (without thermal conduction losses) is shown in Fig. 4 for a range of T_{EQ} . Figure 5 depicts the dependence of Q on T_{EQ} for a range of τ_B/τ . These

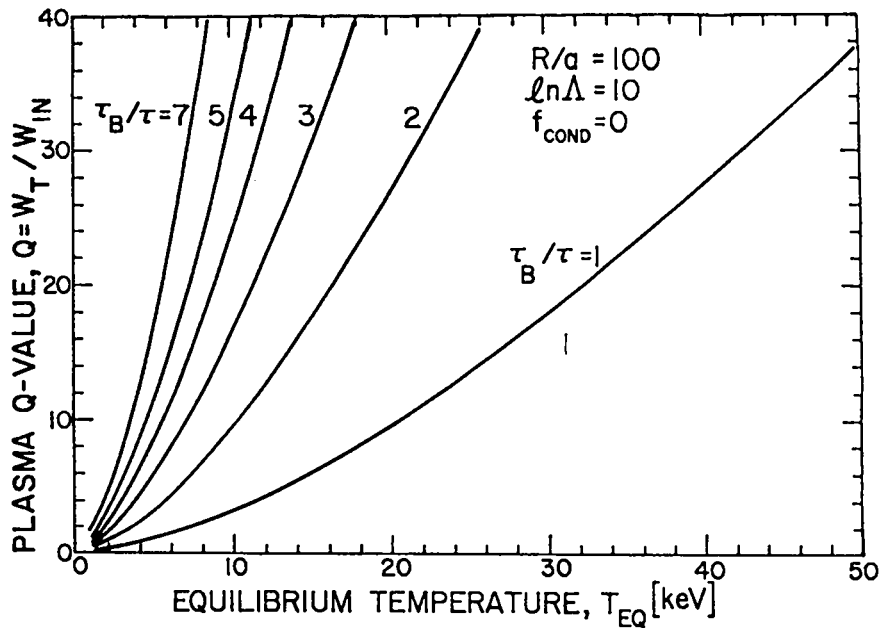


Fig. 5.

Dependence of the plasma Q-value on T_{EQ} and τ_B / τ as given by Eqs. (20), (26) and (29).

results show that a high Q (greater than 20) can be obtained for moderate values of T_{EQ} and τ_B / τ . These prognoses, however, must be tempered by a number of physical constraints, as discussed below.

E. Physics Constraints and Preliminary Design Point Evaluation

Before the scaling relationships derived in the previous section can be evaluated, a number of physical constraints, heretofore left unaccounted, must be considered. These constraints are quantified in this section and can be classified as: particle drift effects; fuel burnup and refueling; and trapped field energy decay. Although clearly coupled to these processes, corona and radial-transport phenomena cannot be explicitly treated within the scope of this study.

1. Particle Drifts

Because of thermal motion and presence of a non-uniform magnetic field, B_θ , along the pinch radius, plasma particles will drift out of the plasma column at both the end and lateral surfaces. Expressions for the axial and radial drift velocities can provide an estimate of the minimum plasma size required for a fusion reactor, although end effects at electrodes will and

have been assumed to play a major role²¹ in ameliorating the effects predicted by this simple analysis.

First, the plasma radius, a , must be much greater than the mean ion Larmor radius, r_L , in order to limit ion orbit losses. The complex role that such orbit effects play in creating and sustaining a corona region in the dense surrounding gas is recognized but ignored by this simple analysis.

The ion Larmor radius is given by

$$r_L = mv_{\perp}/eB \quad , \quad (32)$$

where v_{\perp} is the velocity component perpendicular to the magnetic field lines. Replacing v_{\perp} by $(2k_B T/m)^{1/2}$ and B by the volume-averaged value $\langle B_{\theta} \rangle = (2/3) B_{\theta 0} = (2/3) \mu_0 I/2\pi a$, Eq. (32) transforms into the following expression.

$$r_L = 3\pi a(2mk_B T)^{1/2}/e\mu_0 I = 0.025aT_{EQ}^{1/2} \quad . \quad (33)$$

Consequently, for temperatures in the range 5 to 30 keV, the ratio r_L/a lies in the acceptable range of 0.06 to 0.14.

In evaluating plasma length constraints, a condition can be drawn from the gradient-B drift motion and centrifugal acceleration resulting from the nonuniformity of the magnetic field. The drift occurs in the axial direction and is characterized by a velocity, v_D , given by

$$v_D \approx [2W_{\parallel}/r - W_{\perp}|\nabla B|/B]/eB \quad , \quad (34)$$

where $W_{\perp} \sim W_{\parallel} = k_B T$. Using the approximation $|\nabla B| \approx B_{\theta 0}/a$, $r \approx 2a/3$ and $B \approx \langle B_{\theta} \rangle = 2B_{\theta 0}/3$, as well as Eqs. (32) and (33), Eq. (34) becomes

$$v_D(\text{m/s}) \approx 9(10)^7 k_B T / (8eI) = 8272\theta^{1/2} T_{EQ} \quad . \quad (35)$$

If ℓ is the length of the plasma column, the constraint that the drift time, $\tau_{DR} \equiv \ell/v_{DR}$, must be longer than the burn time, τ_B , imposes a minimum value for the pinch length, ℓ . This constraint is given by

$$\ell(m) > v_D \tau_B = 8272 \theta^{1/2} \xi \tau_{EQ} = 5,57(10)^{24} \xi T_{EQ}^{3/2} / \langle n \rangle \equiv \ell_{min} \quad , \quad (36)$$

where, again, $\xi = \tau_B/\tau$. For a given plasma density, the minimum length, ℓ_{min} , is proportional to $T_{EQ}^{3/2}$; for a given temperature T_{EQ} , ℓ_{min} is proportional to a^2 . As an example, T_{EQ} and Q are assumed, respectively, to equal 8.5 keV and 30; this value for Q corresponds to an engineering Q -value of ~ 7 , as is shown in Sec. IV. According to Eqs. (29), (26) and (20), $\xi = \tau_B/\tau$ must equal 5.6. On the other hand, a temperature T_{EQ} of 8.5 keV corresponds to a line density of $3.4(10)^{19} \text{ m}^{-1}$, as predicted by Eq. (15). Furthermore, it is supposed that a 0.05-mm-radius plasma column can be produced; in this case the minimum length, ℓ_{min} , will be 0.19 m.

Within one limit the particle/energy losses associated with the axially-directed particle drift could be compensated by refueling and ohmic heating. In this case the energy balance, Eq (7), must be re-written according to

$$\frac{d}{dt} (3 \langle n \rangle k_B T) = f_\alpha P_\alpha + P_{OHM} - P_{BR} - P_{COND} - P_{DR} - 2 \langle n \rangle k_B T (d \ell n a^2 / dt) \quad , \quad (37)$$

where the drift losses are approximated by

$$P_D = 3 \langle n \rangle k_B T / \tau_{DR} = 368 T \theta^{1/2} / \ell a^2 \quad . \quad (38)$$

Unfortunately, the added drift term makes impossible the transformation of the energy-balance equation into a simple analytic expression that is similar to Eq. (17). Nevertheless, the power loss represented by P_{DR} could be significant and may preclude appreciable ohmic heating of the plasma column. The experimental fact, however, is that significant heating in the presence of electrodes can be achieved, and the simple treatment leading to Eq. (38) must

be viewed as highly pessimistic. Mass motion related to axial drifts may occur to an extent allowed by axial pressure balance against fixed electrodes, and energy will be drained from the plasma column by axial thermal conduction in a constant-mass pinch. Axial cross-field diffusion of thermal energy, however, can be shown²¹ to be unimportant in the classical limit. Consequently, the dire predictions of this simple drift approximation for axial loss is considered an overly pessimistic estimate and is ignored by the subsequent reactor analyses. The question of radial thermal conduction is addressed, however, by the zero-dimensional and one-dimensional DZPR burn codes (Sec. IV and Appendix B, respectively).

2. Alpha-Particle Containment

Unlike many fusion schemes, significant alpha-particle heating of the DZP appears to be undesirable. As has been shown by numerical burn simulations (Sec. VI), the intrinsic coupling between the ohmic heating and the pressure/particle confinement makes any additional heating highly undesirable from the viewpoint of constant or nearly constant radius operation. Even a small amount of alpha-particle heating will disrupt this delicate pressure balance, causing a rapid expansion of the current channel, premature disassembly of the plasma column and a decrease in the total thermonuclear yield; a correspondingly poor system Q-value results. The issue of alpha-particle confinement in small radii plasma columns has been addressed briefly within the context of the Fast Liner Reactor,²¹ and, although not fully resolved, indications exist that for sufficiently short columns the high-energy alpha particles should rapidly drift axially out of the plasma by a mechanism similar to those described previously in Sec. III.E.1. The radial extent of the 3500 keV alpha particle, at peak DZP current, I_{EQ} , however, is such that $r_{L\alpha}/a \approx 1.5$, according to Eq. (33). Consequently, alpha-particle energy is expected to be deposited within the coronal periphery of the plasma column, contributing to transport processes associated with this region of the DZP. As noted previously, this aspect of the DZPR could not be analyzed quantitatively within the scope of this study. Generally, both analytical and numerical computations assume all alpha-particle energy is deposited external to the plasma column.

3. Fuel Burnup/Depletion

If the plasma column is not replenished with fresh DT, fuel limitations will place a constraint on the maximum fusion yield, W_T (J/m), as given by Eq. (28). Designating the fuel burnup fraction by f_B , W_T without refueling must equal $1.6(10)^{-12} N f_B$, where N is the line density, $\langle n \rangle \pi a^2$. Equating W_T to this burnup limit and using Eq. (15) for T_{EQ} , the following burnup constraint results

$$f_B N^{5/2} / (\tau_B / \tau - 1) = 2.25(10)^{45} (\ln \Lambda)^{5/2} \quad . \quad (39)$$

For a given burnup fraction, f_B , and normalized burn time, $\xi = \tau_B / \tau$, the burnup constraint places a definite constraint on the line density, N . Furthermore, Eq. (29) for Q , when expressed in terms of N , takes the following form

$$Q = 1.30(10)^{-19} (\ln \Lambda)^{2/3} N / [\ln(R/a) + 0.25] \quad . \quad (40)$$

Using Eqs. (39) and (40), regions in Q versus T_{EQ} space (Fig. 5) and W_T versus $\xi = \tau_B / \tau$ space (Fig. 4) can be eliminated for a given value of f_B . Figures 6 and 7 illustrate the burnup constraint on Q and W_T , respectively, for $\ln \Lambda = 10$ and $f_B = 0.5$. Other limiting values of f_B can be evaluated, according to Eqs. (39) and (40) by an appropriate scaling, although $f_B = 0.5$ represents a point of diminishing returns for any unrefueled, binary reaction. In terms of maximizing the system Q -value, the burnup constraint clearly forces the system to lower temperatures, T_{EQ} , and extended burn times, $\xi = \tau_B / \tau$. Increasing f_B raises the burnup constraint depicted on Figs. 6 and 7. It is noted that the burnup constraint is based upon the approximation that $g(\theta) \approx \xi - 1$, which is valid only for $\theta \approx 1$ or $\xi = \tau_B / \tau \gg 2-3$. Finally, it is emphasized that the construction of this burnup constraint is predicted on the assumption of no neutral gas ingestion and transport from the surrounding high-pressure reservoir into which the DZP is embedded; only more detailed analyses will resolve this issue, although the f_B constraint can be considered as conservatively pessimistic.

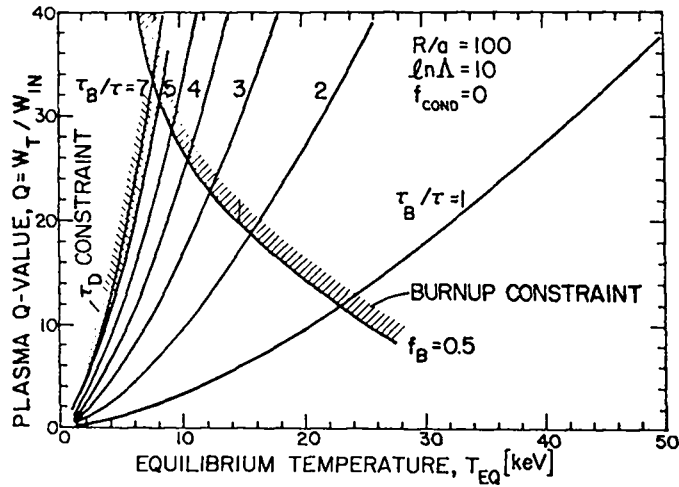


Fig. 6.

Dependence of plasma Q-value on T_{EQ} and τ_B / τ , showing burnup and energy-replacement constraints.

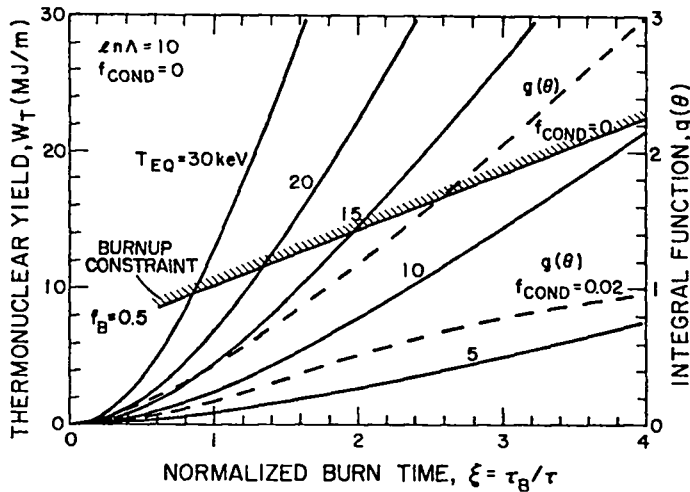


Fig. 7.

Dependence of thermonuclear yield, W_T , on T_{EQ} and τ_B / τ , showing burnup and energy-replacement constraints.

4. Energy Replacement

Implicit in the derivation of this simple DZP model is the assumption that the ohmic heating energy can be supplied to the system by external means and that the field energy, W_B , remains constant throughout the burn phase. In actuality, however, the electrical system may be "crowbarred", and the ohmic dissipation should be reflected by a decay of current and magnetic field. A resistive decay time, τ_D , is defined to quantify this "energy-replacement" constraint

$$\tau_D = W_B/P_{OHM} = 3.03 [\ln(R/a) + 0.25] T^{3/2} \pi a^2 \quad . \quad (41)$$

Unless $\tau_B < \tau_D$, energy must be supplied to sustain the DZP current. Similar to the burnup constraint, application of the energy dissipation constraint, $\tau_B < \tau_D$, represents a convenient means to focus the search for attractive DZP parameters; application of these constraints to this study does not necessarily infer that a means of circumvention cannot be found.

Applying Eqs. (15) and (41) to the energy depletion constraint gives the following constraint on τ_B/τ

$$\xi = \tau_B/\tau < 0.13 [\ln(R/a) + 0.25] \ln \Lambda \quad . \quad (42)$$

Hence, for $R/a \approx 100$ and $\ln \Lambda \approx 10$, ξ must be less than 6.4. This energy replacement constraint is also depicted on Fig. 6, which, when applied in conjunction with the $f_B \approx 0.5$ constraint, infers that $N < 3.57(10)^{19} \text{ m}^{-1}$, $T_{EQ} > 8.2 \text{ keV}$ and $Q \lesssim 30$.

5. Preliminary Physics Operating Point Based upon Analytic Model

As a consequence of the foregoing analyses, the simple analytic model, when evaluated in conjunction with f_B and τ_D constraints, can be used to specify a surprisingly narrow range of DZPR physics operating points. Selecting $f_B = 0.5$, $R/a=100$, $\ell = 0.1 \text{ m}$ and $\ln \Lambda = 10$, and designating $Q = 20$, 30, or 40 allows three possible DZPR parameter lists to be constructed.

Table II summarizes these potential operating points; the N value results from the f_B constraint for a given Q -value (Eq. (40)), and the T_{EQ} value results from Eq. (15). Within any of these three cases, a range of subcases are indicated that depend upon the exact value selected for the DZP radius, a . Once the radius is selected, the average density, $\langle n \rangle$, and burn time, τ_B , result. It is noted that the $Q = 40$ case violates the τ_D constraint ($\xi < 6.4$); the $Q = 30$ case represents an optimal case if both the f_B and τ_D constraints are enforced.

The predictions embodied in Table II should be taken only as indicative, and a more detailed plasma/circuit model, described in the following section, is actually used to generate a specific DZPR parameter list. Nevertheless, these predictions appear both realistic and encouraging, particularly from the viewpoint of the estimated magnitudes of τ_B , τ (circuit rise time), Q , and $W_B \ell$. This optimism hinges significantly on the ability to achieve a nearly constant radius burn for plasma radii in the sub-millimeter range indicated in Table II.

TABLE II
SAMPLE DESIGN POINTS ASSUMING BATCH BURN (a)

Q	20		30		40	
N ($10^{19}/m$)	2.25		3.37		4.5	
T_{EQ} (keV)	12.9		8.65		6.5	
W_T (MJ)	1.8		2.7		3.6	
τ_B/τ	2.70		5.6		10.6	
a (μm)	50	100	50	100	50	100
$\langle n \rangle$ ($10^{27}/m^3$)	2.9	0.72	4.3	1.1	57	1.4
τ_B (μs)	2.3	9.2	2.6	10.4	3.2	12.6

(a) based on $f_B = 0.5$, $R/a = 100$, $\ell = 0.1$ m, $\ell n \Lambda = 10$ for $I_{EQ}(\text{MA}) = 1.36$ and $W_B \ell (\text{MJ}) = 0.09$.

IV. DETERMINATION OF PHYSICS OPERATING POINT

Analytic calculation of the DZPR time response, as described in Sec. III, imposed the constraint of maintaining a constant plasma radius; operation at the Pease current during the burn was required. The desirability of this operating mode is open to question when attempting to maximize the overall system Q-value. Operation at the Pease current may also be difficult to achieve when the realities of the electric circuitry are properly taken into account. This situation is especially applicable when nonlinear effects, such as resistive decay of the current, fuel burnup, alpha-particle heating, and particle/heat losses are included. A time-dependent burn code, therefore, is used to evaluate the general problem of DZPR operation with a time varying plasma radius. Before describing this zero-dimensional plasma model and associated results, however, a generalized DZPR engineering energy balance is formulated to relate the plasma Q-value, Q , to the engineering Q-value, Q_E , and other important system parameters.

A. Engineering Energy Balance

Considering electricity production using a DZPR, the engineering Q-value, Q_E , defined as the inverse of the recirculating power fraction, $\epsilon = 1/Q_E$, can be deduced from a generalized energy flow diagram depicted in Fig. 8. The energy input, W_{IN} , delivered to the plasma as magnetic field and plasma kinetic energy vis a vis ohmic dissipation results in a thermonuclear energy

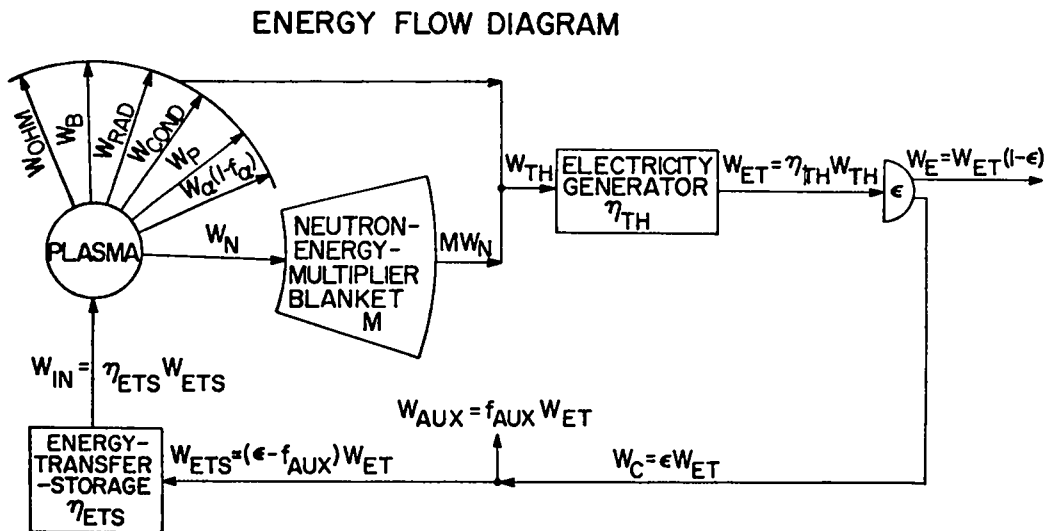


Fig. 8.
Generalized engineering energy flow and power balance for the DZPR.

release, $W_T = W_N + W_\alpha$, associated with the fusion neutrons, W_N , and alpha particles, W_α ; a fraction f_α of the alpha-particle energy is assumed to remain in the plasma. The exoergic nuclear reactions in the blanket amplify the neutron energy by a factor M . The total thermal energy, W_{TH} , is transformed into electrical energy, W_{ET} , with an efficiency η_{TH} . A portion $\epsilon = 1/Q_E$ of W_{ET} is recirculated to supply all DZPR power requirements; a fraction f_{AUX} of the total electrical energy is used for auxiliary needs, and the remainder is used to create the pinch through an energy transfer-storage system having an efficiency η_{ETS} . Consequently,

$$Q_E \equiv 1/\epsilon = W_{ET}/W_C = \eta_{TH} W_{TH}/(f_{AUX}W_{ET} + W_{ETS}) \quad (43)$$

Assuming both radial and axial plasma losses are recovered as thermal energy,

$$W_{TH} = MW_N + W_\alpha + W_{IN} \quad (44)$$

Using a definition of Q similar to that given by Eq. (27), but which is not dependent explicitly on the blanket energy multiplications, M

$$Q = W_N(1+W_\alpha/W_N)/W_{IN} \quad (45)$$

Eq. (43) can be written to give an explicit relationship between Q_E and Q

$$Q_E = \frac{\eta_{TH}\eta_{ETS}\left[1 + Q \frac{M+h}{1+h}\right]}{1 + f_{AUX}\eta_{TH}\eta_{ETS}\left[1 + Q \frac{M+h}{1+h}\right]} \quad (46)$$

where $h = W_\alpha/W_N = 3.5/14.1 \approx 0.25$, and, typically M is in the range 1.1 to 1.2. Figure 9 graphically displays the dependence of Q_E on Q for three sets of M , η_{TH} and η_{ETS} values that are identified as pessimistic, nominal, and

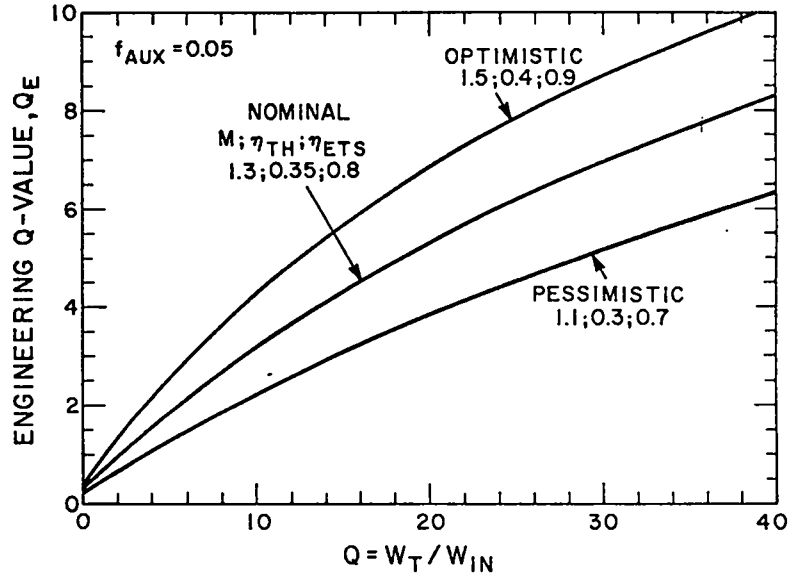


Fig. 9.

Parametric evaluation of Eq. (46) showing the dependence of engineering Q-value, Q_E , on the plasma Q-value, Q , for three sets of values of the blanket multiplication, M , the thermal-to-electric conversion efficiency, η_{TH} , and the energy transfer and storage efficiency, η_{ETS} .

optimistic. From the viewpoint of economics, Q_E values much below ~ 5 are undesirable; consequently, values of Q in the range 15-30 are required. It is noted that since M and η_{TH} are expected to vary only over a narrow range, the transfer efficiency, η_{ETS} , represents a primary parameter in setting the required Q , given that $Q_E > 5$. In the spirit of this Level III study, therefore, the focus falls onto a parametric evaluation of Q , with Fig. 8 or Eq. (46) serving as the primary connection between Q and Q_E .

B. Description of Numerical Point Model

The time-dependent point model solves the equivalent of Eqs. 1-14 given in Sec. III for a three-particle (electrons, ions, alpha-particles) system. Enforcing pressure balance and integrating over an assumed isothermal plasma cross-section allows the use of spatially-averaged parameters for the numerical simulation of burn dynamics. The DZPR code performs a consistent calculation of a multi-species plasma while following the plasma radius with time in conjunction with voltages and currents in the plasma and associated electrical circuitry. Alpha-particle thermalization can be modeled by a Fokker-Planck formalism, ohmic heating is based on classical resistivity, radiation (Bremsstrahlung, cyclotron) losses are included, and radial thermal

conduction and particle diffusion are approximated. The point DZP plasma model is similar to the RFPR model described in Appendix A of Ref. 23.

A complete time-dependent circuit model is evaluated simultaneously with the thermonuclear burn simulation in which a Marx capacitor bank is used to charge a water-filled transmission line that in turn is discharged into the nonlinear plasma load. The plasma current is "crowbarred" after reaching a maximum value, and the current is allowed to decay resistively for the duration of the burn. The use of a power crowbar to sustain the burn has not been considered; extended burns may be possible, but the assumption of unrefueled burns and importance of coronal transport must be re-examined before this mode of DZPR operation is considered. Specifically, the following assumptions were invoked when utilizing the point DZPR computer model:

- Stability of the cylindrical plasma column is presumed for all computations.
- Estimates of ohmic heating are based on classical resistivity and uniform current density in the pinch.
- All alpha particles are assumed lost instantaneously from the plasma with no energy deposited in the plasma column.
- Only Bremsstrahlung and cyclotron radiations are included; all other radiative and conductive losses are assumed to be negligible.
- Pressure balance is enforced at all plasma radii, and radially averaged plasma parameters are used. An isothermal plasma column supporting a parabolic density profile and a uniform current is used to compute these averages.
- Neither the coronal processes, shock formation in the dense gas, nor peripheral diffusion of plasma are taken into account; therefore, only a batch-burn (unrefueled) operation is considered by these analyses.

C. Parameter Study

An optimization study was first performed using the DZPR code in order to establish the scaling of Q with plasma parameters and to estimate a reactor operating point. Experimentally achievable¹⁷ starting radii of 10^{-4} m were used with an arbitrarily selected pinch length of 0.1 m. The Marx-bank/water-line driving circuit (Sec. V.B) was matched by trial-and-error methods to the plasma load such that energy transfer was achieved with nearly 95% efficiency. The plasma Q-value was then evaluated for a range of driving circuit energies, W_{MARX} , and line densities, N. The results from this

comprehensive parameter search are summarized in Fig. 10. These results virtually depend on no other variables than those shown and, therefore, represent "universal" design curves that are limited only by the modelistic assumptions.

The energy of the driving circuit was adjusted by varying the initial voltage, V_{MARX} , applied to the Marx bank. For all cases shown in Fig. 10 the plasma current rises to a maximum in $0.31 \mu\text{s}$, is crowbarred and subsequently is allowed to decay resistively for $4.69 \mu\text{s}$ ($\tau_B = 5 \mu\text{s}$). The time-dependent behavior of key plasma parameters for an optimal case is described in Sec. IV.D.

The sharp Q-value optima exhibited in Fig. 10 are characterized by high plasma burnup (0.8-0.9) and elevated final temperatures ($\sim 40 \text{ keV}$). Decreasing the line density below the optimum lowers the Q-value approximately linearly with line density, N . Increasing the line density above the optimal value results in a lowering of the plasma temperatures; a faster current decay

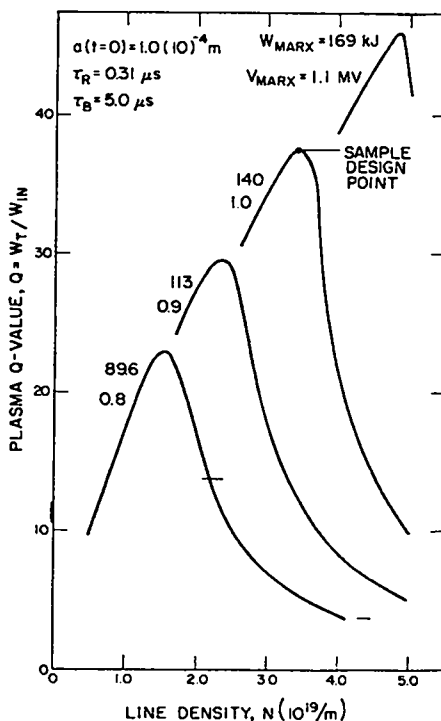


Fig. 10.

Dependence of the plasma Q-value on plasma line density and driving-circuit energy and voltage. For all cases the current rise time was tailored to $0.31 \mu\text{s}$ and the peak current was crowbarred for $4.69 \mu\text{s}$, giving a total burn time of $5.0 \mu\text{s}$.

and lower plasma burnup ensues, causing the decrease in Q . These results appear to be relatively insensitive to the assumed current risetime or the crowbar time, primarily because of the assumption of batch burn and the high fuel burnup.

D. Physics Design Point

As for any highly-pulsed conceptual fusion reactor, the DZPR should achieve an adequate Q -value while minimizing the output energy per pulse in order to alleviate the energy transfer/storage and blast containment problems. From the parametric evaluations given in Sec. IV.A. and on Fig. 9, a $Q \geq 30$ is considered attractive. Consequently, the 1-MV discharge is chosen from Fig. 10 as a sample DZPR design point. The time behavior of the fractional plasma burnup, f_B , electron, T_e , and ion, T_i , temperatures, plasma current, I , and plasma radius, a , is shown in Fig. 11. After 2 μ s, the fuel burnup for this case was computed to be 0.81; much longer burn times and refueling are

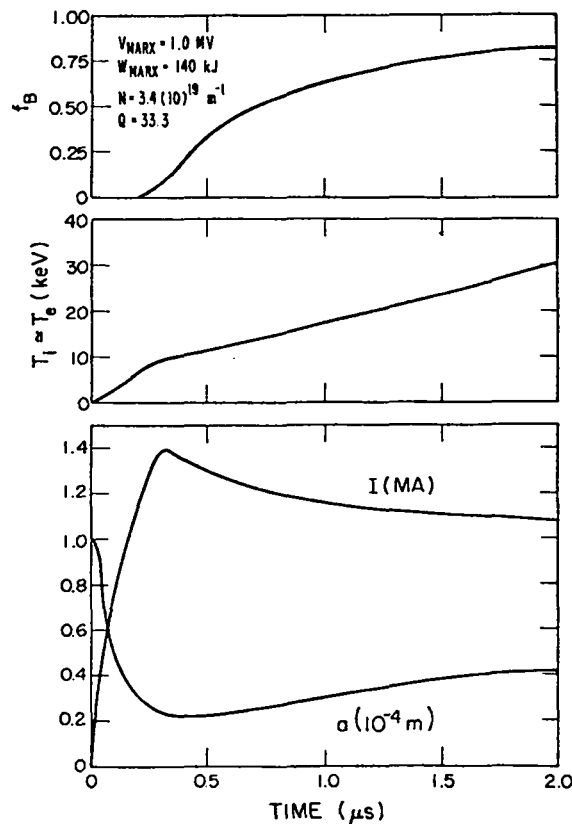


Fig. 11.
Time-dependence of plasma burnup fraction, temperature, current, and radius for a design point corresponding to $Q = 33$, $V_{MARX} = 1$ MV from Fig. 10.

required to achieve any appreciable increases in Q above the value of 33 computed for this design point. This behavior is illustrated by a plot of the plasma powers given in Fig. 12. At 2 μs into the burn the alpha-particle power is reduced to only 10% of the peak level. The burn time for this case, therefore, is taken to be 2 μs with a resultant Q -value equal to 33.3; this result compares to a Q of 38 for the longer 5- μs burn plotted in Fig. 10.

As seen in Fig. 11, the plasma current rises to 1.45 MA in 0.31 μs . A current of 1.45 MA slightly exceeds the Pease current limit and results in a plasma compression from a radius of 10^{-4} m to $0.3(10)^{-4}$ m. This compression heats the plasma and leads to a shorter burn time because of the higher resultant particle density and fusion reactivity. After being crowbarred at 0.31 μs , the current resistively decays for the duration of the 2- μs burn. The ohmic heating associated with this resistive decay causes the plasma temperature to increase continually, and the plasma radius expands slowly as the current falls below the Pease current; as seen from Fig. 12, eventually

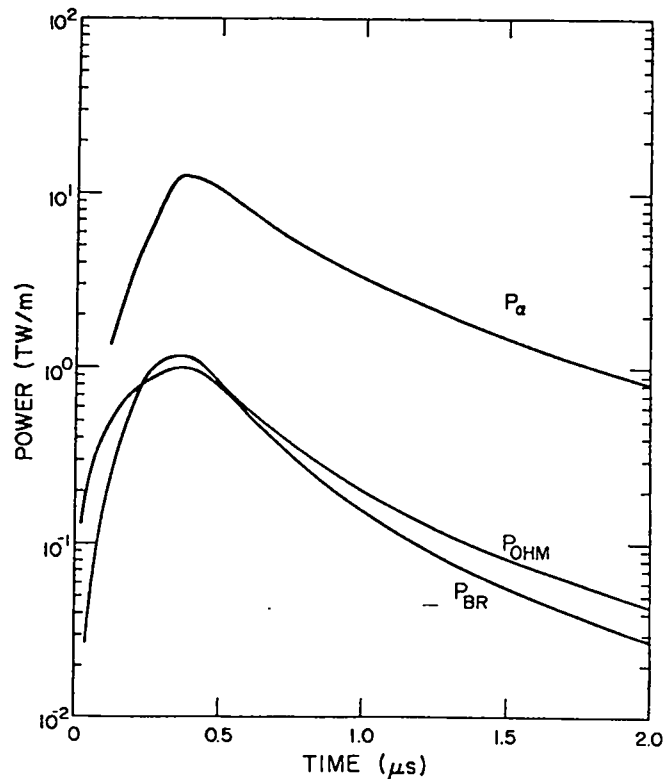


Fig. 12.

Time dependence of alpha-particle, ohmic, and radiation powers for a sample design point.

the ohmic power again exceeds the radiation losses. The plasma density correspondingly decreases as the burnup increases because of the assumed absence of coronal refueling and the complete loss of alpha particles. A summary of key reactor parameters for the operating conditions depicted on Figs. 11 and 12 is given in Table III.

Before concluding this section and accepting the parameters listed in Table III as a typical but interim DZPR design point, it is advisable to compare the predictions of the numerical plasma/circuit model with those projected by the analytic model evaluated in Sec. III. Unfortunately, a direct quantitative comparison is not possible because of inherent modelistic assumptions; the analytic model is based on operation at the Pease current limit, whereas the numerical model predicts operating both above and below the 1.36-MA ($\ln A = 10$, Eq. (19)) Pease current, while still maintaining a relatively constant plasma radius once the initial decrease from $1.0(10)^{-4}$ m to $0.3(10)^{-4}$ m occurs (Fig. 11). Using the line density from Table III, Eq. (15) would predict $T_{EQ} = 8.3$ keV, whereas, the numerical results given in Fig. 11 shows that an equilibrium temperature is not reached over the span of the $\tau_B = 2.0$ - μ s burn period because of the crowbarred resistive decay. Evaluation of the time constant τ (Eq. (16)) is made ambiguous because of the radius variation depicted in Fig. 11. If the initial value of $a = 1.0(10)^{-4}$ m is taken, then $\tau = 1.80$ μ s ($\xi = \tau_B/\tau = 1.1$), or, if an average value of $a = 0.35(10)^{-4}$ m is taken, then $\tau = 0.22$ μ s ($\xi = 9.1$). Use of Figs. 4 and 5 to estimate W_T and Q would give 2.5 MJ/m and 2.0, respectively, if the initial plasma radius is used, and considerably higher values for W_T and Q would result if the average plasma radius is used. Although the claim can be made that "the truth lies somewhere in between", in actuality a quantitative comparison between these significantly different operating modes (i.e., plasma models) is probably unwarranted. Perhaps the major value of this comparison rests with the conclusion that constant radius operation is not particularly desirable from the viewpoints of both the circuit requirements and the system energy balance; this conclusion is very sensitive to the assumed line density, however, (Fig 10). If a comparison case is to be identified for the analytical model, the $Q = 30$, $a = 0.5(10)^{-4}$ m case summarized in Table II is probably more representative of the numerical case given in Table III. Appendix B compares the results of this zero-dimensional burn model with a radial MHS burn model.

TABLE III
SUMMARY OF DZPR DESIGN PARAMETERS

<u>PARAMETER</u>	<u>VALUE</u>
Line density, $N(10^{19}/m)$	3.4
Lawson parameter, $\langle n\tau \rangle (10^{21} \text{ s}/m^3)$	9.75
Fractional burnup, f_B	0.81
Initial plasma radius, $a(10^{-4}m)$	1.00
Plasma length, $l(m)$	0.1
Return-current conductor radius, $R(m)$	0.005
Plasma current risetime, $\tau_R(\mu s)$	0.311
Burn time, $\tau_B(\mu s)$	2.0
Maximum plasma current, $I (MA)$	1.45
Input Marx-bank energy, $W_{MARX} (kJ)$	240
Energy transfer efficiency, $\eta_{ETS}^{(a)}$	0.95(a)
Thermonuclear yield, $W_T (MJ)$	4.4
Plasma Q-value, $W_T/\eta_{ETS}W_{MARX}$	33.3
Assumed thermal conversion efficiency, η_{TH}	0.35
Assumed blanket multiplication, M	1.17
Auxiliary power fraction, f_{AUX}	0.05
Engineering Q-value, Q_E	7.85
Recirculating power fraction, $\epsilon = 1/Q_E$	0.13

(a) actually computed from realistic circuit/plasma parameters(Sec. V.A)

V. PRELIMINARY ENGINEERING CONSIDERATIONS

The nature of this Level III study has not permitted detailed consideration to be given to engineering technology issues anticipated for the DZPR. Nevertheless, certain engineering technology issues could not be totally ignored. Specifically, the power supply and the general reactor configuration have been subject to preliminary examination and are qualitatively addressed in this section.

A. Voltage and Power Supply Requirements

The DZPR thermonuclear burn code described in Sec. IV.B also performs a complete circuit analysis in which the Marx capacitor bank charges a water-filled transmission line that in turn is switched into and drives the time-varying plasma load. The circuit consists of a number of basic circuit modules, as illustrated in Fig. 13, that are connected in parallel. The Marx bank and water line are modeled by setting R_1 and R_2 , respectively, to a large and a small value, with the water line simulated by 40 parallel connected circuit modules of the kind depicted in Fig. 13. Setting R_1 to a large value and C to a small value, the plasma can be modeled by shorting R_2 to ground

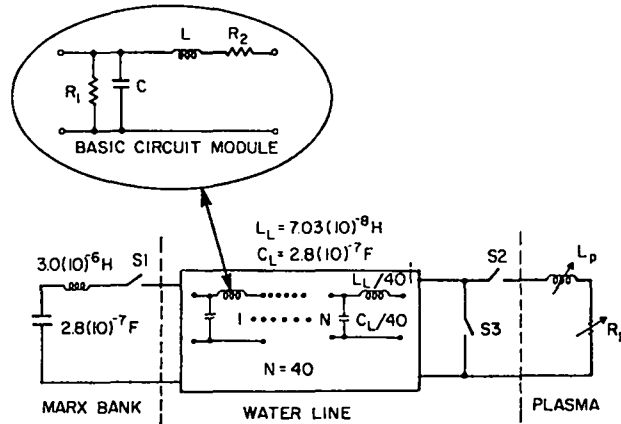


Fig. 13.

Circuit model used in conjunction with plasma model to simulate the DZPR burn.

potential. The equivalent circuit used to model the DZPR is also illustrated in Fig. 13.

Specifying the energy to be delivered to the pinch defines the Marx bank capacitance from the relationship $W_{IN} = 1.4(10)^5 \text{ J} = 0.5 C V_{MARX}^2$, where the voltage $V_{MARX} = 1.0 \text{ MV}$ is given as an input variable. Taking the capacitance of the water line as equal to that of the Marx bank results in a charging voltage, V_L , applied to the water line that equals V_{MARX} . The impedance, Z_L , of the water line is given by $Z_L = \sqrt{L_L/C_L}$, and an upper limit on the load current is given by V_L/Z_L . Because of the nonlinear plasma load, the water-line inductance required to give a desired load current must be found by a trial-and-error procedure. A water-line impedance of 0.5Ω gives a maximum load current of 1.45 MA . Taking the inductance of the Marx bank to be considerably greater than L_L makes the charging time of the water line considerably longer than the discharging time into the plasma load. This relative isolation of the Marx bank allows nearly all of the energy to be delivered to the load during water-line discharge, and only a small fraction of the energy rings back into the Marx system. The discharge time of the water line is approximated by $\tau_R \approx 2\sqrt{LC} \approx 0.28 \mu\text{s}$, which is actually found to be $0.311 \mu\text{s}$ by the numerical simulation.

The switching sequence and time response of the electrical drive described by Fig. 13 is depicted in Fig. 14. Closing switch S1, the water line is charged to $\sim 1.0 \text{ MV}$ in $1.8 \mu\text{s}$. Switch S2 is subsequently closed, and the water line discharges into the plasma load. When the plasma current

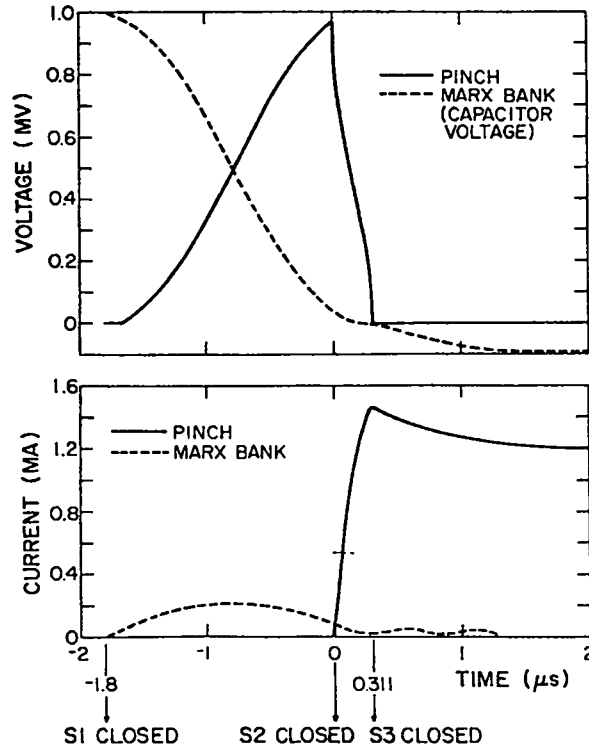


Fig. 14.
Time response of electrical circuit depicted in Fig. 13.

reaches a maximum, switch S3 is closed, and the "crowbarred" current decays through the time-varying plasma resistance, as computed by the thermonuclear burn model. An energy transfer efficiency of 95% is predicted by this complete numerical simulation.

The physical characteristics of a coaxial water line can be evaluated from the following formulae

$$C = 2\pi\epsilon l_w / \ln(r_o/r_i) \quad (47A)$$

$$L = \mu_o l_w / [2\pi \ln(r_o/r_i)] \quad (47B)$$

$$l_w = \sqrt{LC} / \mu_o \epsilon \quad , \quad (47C)$$

where r_o and r_i are the inside and outside coax radii, respectively, and l_w is the length of the water line. The value of ϵ for water is $80\epsilon_o$ where

TABLE IV
DRIVING CIRCUIT PARAMETERS

PARAMETER	VALUE
Marx/water-line charge voltage V_{MARX} (MV)	1.0
Marx/water-line energy W_{MARX} (kJ)	140
Water-line impedance, Z_L (Ω)	0.5
Charge time, τ_C (μs)	1.8
Discharge time, τ_R (μs)	0.311
Length of water line, l_W (m)	4.71
Coaxial water-line dimensions, r_o/r_i (a)	1.077
Outer radius of water line, r_o (m)	0.96
Inner radius of water line, r_i (m)	0.89
Energy transfer efficiency, η_{ETS}	0.95

(a) based on 13.5 keV/mm dielectric strength for water.

$\epsilon_0 = 10^{11}/36\pi$. A summary of the driving circuit parameters is given in Table IV.

B. Reactor Configuration

No detail consideration was devoted to the conceptual design and arrangement of key reactor core components. Although a higher Level II study is required to elucidate these issues, the Marx/water-line configuration to which is affixed the DZP clearly will lead to a number of design and operational constraints. Since both the transferred and fusion energies are small, the issue of a high repetition-rate Marx/water-line system should be less critical than that for systems requiring 1-10 MJ transfers. Furthermore, the low total yields (4-5 MJ) should significantly ameliorate the blast-confinement problem that proves so important for higher-yield devices.²¹ The ~ few MJ yields, however, correspond to only a few cents of revenue per discharge, and more detailed engineering considerations must be given to the quantitative estimate of destroyed material (if any) and the associated replacement cost. Finally, the low thermonuclear releases per discharge will require either a high repetition rate ($> \text{kHz}$) or multichannel (parallel) discharges if reactor systems are to operate in the 100-1000 Mwt regime.

VI. SUMMARY CONCLUSIONS AND RECOMMENDATIONS

The DZP has been analyzed as a potential fusion reactor concept, with an emphasis being placed upon plasma performance; key technology issues must be addressed on the basis of results presented herein, or extensions thereof.

The prognosis that has evolved from this Level III (Conceptual Physics Design) study is viewed as highly positive but preliminary. It appears that the positive potential of the dense-gas stabilized Z-pinch for the production of high-Q power in a highly compact geometry rests with an ability to drive substantial currents (~ 1.3 - 1.4 MA) stably through an extremely small current channel (30 - 100 μm) on a time scale (~ 0.3 μs risetime, ~ 2 - μs "crowbar" time) that is long compared to MHD and/or shock times. The majority of plasma heating would be provided by ohmic dissipation, although some adiabatic compressional heating may result because of constraints imposed by physical considerations of efficient pulsed-circuit operation.

Although this first assessment of the reactor potential of the DZP has focused primarily upon the generalities of plasma performance and energy balance, the results of this analysis indicate a rare and perhaps unique projection that a high-Q DZPR may be too small in energy/power output. Furthermore, this conclusion is based on a driving electrical circuit that appears to represent a near state-of-the-art technology. Both the constant-radius analytic model and the more detailed plasma/circuit numerical model show reasonable agreement with a more detailed radial MHS model (Appendix B). All three models, however, do not describe axial transport or coronal processes, and, of course, all models presume a stable current filament with magnetic fields and plasma pressure that are always in quasi-equilibrium. Given a stable DZP equilibrium within a dense surrounding gas, this study did not reveal either axial transport or coronal processes that might seriously degrade the projected plasma performance, although considerably more analysis and experiment is needed to resolve these important issues. Specifically, radial transport associated with gas ingestion from a radiation/alpha-particle sustained coronal annulus surrounding the plasma column could present both advantages and disadvantages. Inward transport of cold DT gas could present a means to refuel the plasma column, thereby leading to greater fusion yields and plasma Q-values. The enhanced radial loss, on the other hand, will modify the plasma performance predicted by this study, although the overall effect of radial transport associated with coronal processes on the plasma Q-value is not expected to be significant, given that the presumed MHD stable operation can indeed be achieved. This issue, however, also must be subjected to extensive theoretical and experimental study, particularly insofar as coronal/plasma processes influence and/or

determine the macroscopic stability of a dense-gas-embedded pinch and the potential for an undesirability broadened current channel. Alpha-particle thermalization and transport may play an important role in these processes and for the operation of the proposed DZPR may prove to be particularly important; significant heating of the DZP by alpha particles has been shown by the numerical model to cause a premature disassembly of the plasma column by forcing radial expansion, leading to a low-Q yield.

In summary, the following physics issues require additional analysis in order to assess the credibility of the physics design point projected by this study.

- advancement in the understanding of gross stability limits and/or characteristics of a dense-gas-embedded Z-pinch is needed.
- modeling of coronal processes driven primarily by radiative and alpha-particle transport. Both the potential benefits of gas-blanket refueling and the adverse effects of enhanced radial transport should be examined.
- better modeling of axial transport of energy and mass to and from electrode surfaces is needed.

The level of study devoted to the DZPR assessment was insufficient to permit analyses and estimates of major reactor technology issues. On the basis of the plasma/circuit analyses performed, however, it appears that a water-filled transmission line that is charged by a relatively small Marx bank may represent a highly efficient and straight-forward means to generate and to drive the DZP discharge; this energy transfer/supply system can be small if the projections of plasma performance made by this study are correct. The rapid and frequent switching of ~ 100 -kJ energy levels through these simple, reliable, and conventional power supplies should in themselves require only a straight-forward and modest development effort.

As for other systems of this nature, the "front-end" section of the water-line co-axial conductor will undoubtedly drive all important elements of the reactor technology design. This aspect of the DZPR has received no quantitative attention by this study. If the thermonuclear releases can be preserved at the 1-10 MJ (total) level while maintaining a high-Q (> 30) performance, however, the issue of blast confinement per se should not be serious, if this issue exists at all for the DZPR configuration. The

potential problem related to the amount (if any) and complexity of apparatus that must be destroyed each shot versus the revenue generated by each high-Q discharge, however, remains to be quantified. Finally, the means by which a useful level of power (> 100 MWt) can be generated by the DZPR has not been quantified; this latter issue revolves around allowable pulse frequency versus the number of simultaneous discharges that can be initiated by a single Marx-bank/water-line energy storage/transfer system. Although future design studies could be helpful in resolving these technological questions, it is recommended that the centrum of future activity be placed in the areas of physics uncertainty listed at the beginning of this section.

REFERENCES

1. R. Aymer, C. Etievant, P. Hubert, A. Samain, B. Taquet and A. Torossian, "Experimental Studies of the Pinch Phenomenon," Proc. 2nd UN Conf. on Peaceful Uses of Atomic Energy, (United Nations, Geneva) 32, 92 (1958).
2. O. A. Anderson, W. R. Baker, S. A. Colgate, J. Ise, Jr. and R. V. Pyle, "Neutron Production in Linear Deuterium Pinches," Phys. Rev., 110, 6 1375-1387 (1958).
3. M. N. Rosenbluth, "Stability of the Pinch," Los Alamos Scientific Laboratory report LA-2030 (July, 1959).
4. B. Kadomtsev, "Hydromagnetic Stability," Reviews of Plasma Physics, 2, 153 Consultants Bureau, N.Y. (1966).
5. C. W. Hartman, "High-Density Fusion and the Z-Pinch," Lawrence Livermore Laboratory report UCID-16371 (1973).
6. C. W. Hartman, D. Y. Cheng, G. E. Cooper, J. L. Eddleman and R. H. Munger, "High Density Fusion and the Z-Pinch," Proc. 5th IAEA Conf. on Plasma Physics and Controlled Nuclear Fusion (Tokyo, 1974), 2, 653 (1975).
7. W. M. Manheimer, M. Loumpe and J. B. Boris, "Effect of a Surrounding Gas on Magnetohydrodynamic Instabilities in Z-Pinch," Phys. Fluids, 16, 7, 1126 (1973).
8. D. E. Potter, "Numerical Studies of the Plasma Focus," Phys. Fluids, 14, 9, (1971).
9. C. W. Hartman, "Finite Larmor Radius Stabilized Z-Pinches," Lawrence Livermore Laboratory report UCID-17118 (1976).
10. A. A. Newton, J. Marshall and R. L. Morse, "Observation of Coaxial MHD Plasma Flow," Proc. 3rd Europ. Conf. on Controlled Fusion and Plasma Physics, p. 119 (1969).
11. J. G. Linhart, "Very-High-Density Plasmas for Thermonuclear Fusion," Nucl. Fusion, 10, 211 (1970).
12. J. W. Struve, C. W. Hartman, R. H. Munger and J. W. Shear, "Experimental Studies of Gas-Embedded Z-Pinch Initiated by a Relativistic Electron Beam," Bull. APS, 20, 2, 1296 (1975).
13. R. R. Lindemuth, "Initial Numerical Studies of the Behavior of Z-Pinch Plasma Under Liner Implosion Conditions," Nucl. Fusion, 18, 7, 929 (1978).
14. C. W. Hartman, G. Carlson, M. Hoffman, R. Werner and D. Y. Cheng, "A Conceptual Fusion Reactor Based on the High-Plasma-Density Z-Pinch," Nucl. Fusion, 17, 5, 909 (1977).

15. J. E. Hammel, "An Ohmically Heated High-Density Z-Pinch," Los Alamos Scientific Laboratory report LA-6203-MS (1976).
16. T. A. Oliphant, personal communication, Los Alamos Scientific Laboratory (1979).
17. J. E. Hammel, personal communication, Los Alamos Scientific Laboratory (1979).
18. L. Spitzer, Physics of Fully Ionized Gases, Interscience Publishers p. 105, (1962).
19. S. I. Braginskii, Reviews of Plasma Physics, Consultants Bureau, N.Y. 1, 326, (1965).
20. R. S. Pease, "Equilibrium Characteristics of a Pinched Gas Discharge Cooled by Bremsstrahlung Radiation," Proc. Phys. Soc., 70, 11 (1957).
21. R. W. Moses, R. A. Krakowski, and R. L. Miller, "A Conceptual Design of the Fast-Liner Reactor (FLR) for Fusion Power," Los Alamos Scientific Laboratory report LA-7686-MS (1979).
22. S. Glasstone and R. H. Lovberg, Controlled Thermonuclear Reactor, Van Nostrand Co. p. 79 (1960).
23. R. L. Hagenson, R. A. Krakowski, and G. F. Cort, "The Reversed-Field Pinch Reactor (RFPR) Concept," Los Alamos Scientific Laboratory report LA-7973-MS (August, 1979).

APPENDIX A

Description of DZP Experiment and Comparison of Plasma Model with Experimental Result

A small DZP experiment is operating at LASL.¹⁷ This experiment has two objectives: a) to explore the DZP approach to fusion power, and b) to generate experimental data for the theory of high-density, gas-embedded plasmas. This DZP experiment is briefly described, and typical experimental results are compared to the theory that has served as a basis for the DZPR reactor projection.

The DZP experiment is investigating the feasibility of ohmically heating a filamentary plasma of $\sim 10^{26}$ - 10^{27} m⁻³ density to temperatures of ~ 10 keV. This experiment becomes possible through the use of laser-beam initiation and high-voltage, electron-beam techniques. Figure A-1 gives a schematic diagram of the DZP experiment and lists key system parameters. The experimental configuration is similar to that proposed for the DZPR, using a Marx-bank to charge a water-filled transmission line, which in turn is switched into the plasma load. After initiation of the submillimeter diameter current channel in a dense deuterium gas (~ 1 atm) by a ruby laser beam, the 0.6-MV transmission line provides the 01- μ s current rise time since the current is less than the Pease limit. The present $W_{\text{MARX}} = 5$ -kJ device provides information on the development phase of current channel formation. Currents up to ~ 75 kA can be produced in ~ 0.1 to 1-mm radius pinches.

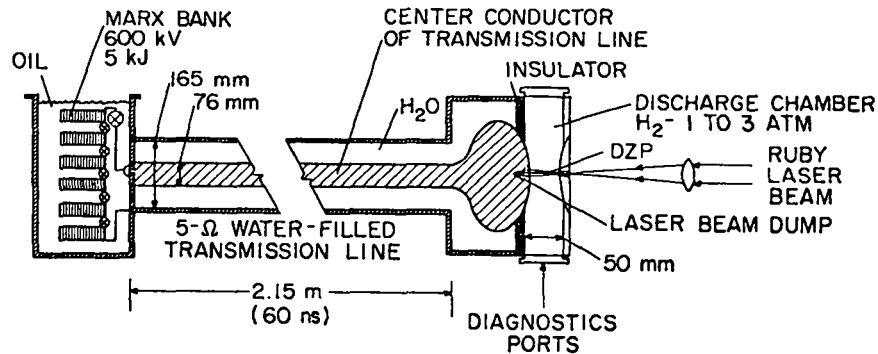


Fig. A-1.

Schematic diagram of LASL DZP experiment, showing important system parameters.

Experiments performed to date show two phases in the current channel formation. First, the ruby laser provides an initially uniform but low-level ionization (i.e., electron seed) path along which the current channel forms. Current channels as small as $0.6(10)^{-4}$ m have been observed experimentally. These channels remain straight and uniform for 30 ns, but the radius expands with time. Figure A-2 gives the time-dependence of both the pinch current and the pinch radius, as measured by Schlieren photography.¹⁷ The measured plasma resistivity indicates a temperature of 40 eV. The second phase of the experiment occurs at times greater than ~ 30 ns, when the current reaches ~ 35 kA. The current channel develops into a tight helix during this second phase. The envelope of the helix remains straight and well-behaved from an MHD viewpoint for the remainder of the 0.12- μ s current pulse.

The emphasis of this experiment is two-fold: the first objective is to achieve pressure equilibrium within the pinch (i.e., to maintain nearly constant the initial column radius) by increasing the voltage in conjunction with a proper switching sequence. The second objective is to investigate the nature of the helical phase under equilibrium conditions.

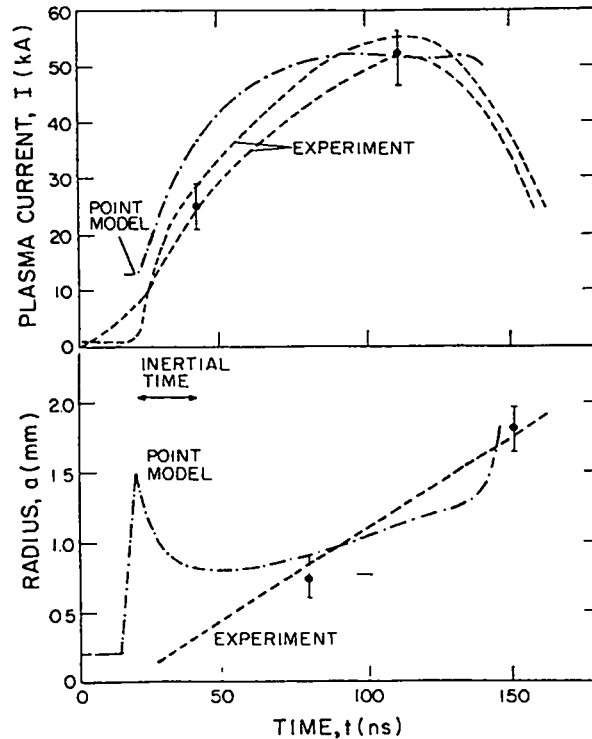


Fig. A-2.
Comparison of theory and experiment¹⁷ for the DZP.

A major reason for including this appendix is to compare the theory used to model the DZPR with experimental data. The computational results from the point plasma model used in the reactor study (Sec. IV) are depicted in Fig. A-2. The point plasma model predicts well the experimentally determined current wave-form, and agreement with the plasma radius trajectory is also good for times greater than inertial times; the initial radial excursion predicted by the point model is expected because this model does not include inertial effects. For the reactor risetime of $\sim 0.3 \mu\text{s}$, inertial terms should not be important, and the point model should be applicable in this regime. A detailed MHD code under development at LASL does treat inertial terms and also shows good agreement with the above experimental results.¹⁶ Neither theory can model the experimentally observed helical phase, however, and it is expected that both theory and reactor projections will be guided by experimental results for some time to come.

APPENDIX B

Description of DZP/MHS* Code and Comparison with Zero-Dimensional Results

The one-dimensional magnetohydrostatic code LNRBRN was developed to model the Fast-Liner Reactor (FLR).²¹ This MHS code system has been modified for application to the dense Z-pinch reactor study. The new revision of this code is called DENSZP and is described in this appendix.

1. DENSZP Plasma Model

a. General Operation

The plasma is treated as a single-fluid gas in cylindrical geometry with an embedded magnetic field, B_0 ; a radially uniform axial current is assumed to establish this embedded field. The DENSZP model computes radial thermal conduction and field diffusion in the MHS approximation. Bremsstrahlung and D-T burnup are computed as functions of radius. Alpha-particle heating of the plasma is not considered, since the alpha-particle mean-free-path for thermalization is several times the plasma dimensions at peak compression. The plasma and field pressures are computed at the plasma-boundary and are dynamically coupled to the driving circuit described in Sec. V.A.

DENSZP is coupled with the same circuits code used with the point plasma model. Since DENSZP cannot model ionization and shock effects that may occur in the early stages of the discharge, a substitute electrical load is coupled initially ($t = 0$) to the circuits code.

It is assumed that the plasma temperature has reached 100 eV and that current is uniformly distributed over the plasma radius before the DENSZP computation begins. The plasma and field are assumed to be in pressure balance according to

$$\mu_0 I^2 / 16\pi = NeT \quad , \quad (B-1)$$

*The term magnetohydrostatic (MHS) is used to describe an MHD approach that neglects inertial terms.

where N is the line density and T is the initial plasma temperature. When current in the initial electrical load representing the plasma reaches the value given by Eq. (B-1), the numerically simulated 100-eV plasma is coupled directly to the circuits code. The electrical circuit model is identical to that described in Sec. V.A.

At each time step, t_k , the plasma resistance, R_p , and inductance, L_p , are passed from DENSZP to the circuits code, where R_p and L_p are given by

$$R_p = \ell \eta_a J_a / I_p \quad , \quad (B-2)$$

$$L_p = \frac{\mu_0 \ell}{2\pi} [0.25 + \ln(R/a)] \quad . \quad (B-3)$$

The quantities η_a and j_a are, respectively, the resistivity and current density at the plasma surface. The circuits code computes a new plasma current for the subsequent time step, $t_{k+1} = t_k + \delta t$, and this current is passed back to DENSZP. In order to compute the time step cycle, DENSZP computes transport and all plasma parameters at time t_{k+1} , matching the plasma current to the value given by the circuits code for time t_{k+1} .

b. Radial Transport

DENSZP is an implicit Lagrangian code. Sound transit times are assumed to be much less than the burn time; inertial terms, therefore, are neglected and plasma motion is determined by a pressure balance ($\vec{J} \times \vec{B} = \vec{\nabla} p$) applied for equal electron and ion temperatures. This MHS pressure balance can be transformed to the following integral equation when the magnetic field possesses only the azimuthal or " θ " direction

$$2nk_B T + B_\theta^2 / 2\mu_0 = (4/r^2) \int_0^r nk_B T r' dr' \quad , \quad (B-4)$$

where e is the Boltzmann constant ($1.6(10)^{-16}$ J/keV), $n(1/m^3)$ is the ion density, $\mu_0 = 4\pi(10)^{-7}$ H.m, and T is expressed in keV units.

Plasma parameters are computed as functions of time by a two-step method.²¹ First, the Lagrangian mesh is fixed in space, and all diffusion and loss processes are evaluated for a given time step. The basic equations are

$$2ne(\partial T/\partial t) = (1/r) \partial [rk\partial T/\partial r]/\partial r + S \quad (B-5)$$

$$\mu_0(\partial B_\theta/\partial t) = \partial [\eta(B_\theta/r + \partial B_\theta/\partial r)]/\partial r \quad (B-6)$$

$$\partial n/\partial t = - n^2 \langle \sigma v \rangle / 2 \quad , \quad (B-7)$$

where k is the thermal conductivity,¹⁹ η is the electrical resistivity,¹⁹ S is a net volumetric power source (or sink), and $\langle \sigma v \rangle$ is the Maxwellian-averaged D-T fusion reactivity. Since the alpha particles are assumed to escape unthermalized from the plasma, charge neutrality requires that two electrons also escape the plasma for each fusion reaction.

The bremsstrahlung power density, as used in the source term S , is taken as²²

$$S_{BR}(W/m^3) = -5.35(10)^{-37} n^2 T^{1/2} \quad . \quad (B-8)$$

After Eqs. (B-5)-(B-7) are solved for a given time step, the Lagrangian mesh is adjusted in space to re-establish pressure balance (Eq. (B-4)), and these equations are then coupled dynamically to the circuit subroutine as previously explained. This procedure completes the two-step approach. Axial particle/energy loss is not modeled by these computations, although an algorithm has been developed to estimate these effects.²¹ For the magnitudes of the magnetic fields and the pinch lengths considered here for the DZPR, these losses are expected to be small, although this assumption warrants more theoretical consideration.

2. Results and Comparisons

The thermonuclear reaction rate for a 50% DT fuel mixture is computed as a function of radial position using tabular values for the D-T, Maxwellian-averaged reactivity, $\langle \sigma v \rangle$. Since the classical alpha-particle mean-free-path is expected to exceed the compressed plasma dimensions, alpha particles are assumed lost and, hence, do not contribute to the plasma energy

or pressure. If a significant portion of the alpha-particle energy were to be retained by the plasma, compression would be inhibited, and the fusion yield is expected to be diminished for the optimized physics operating point reported here.

Figure B-1 compares the predictions of the zero-dimensional model (Case A) described in Sec. IV and the exact replications using identical initial conditions by the one-dimensional MHS model (Case B), including the electrical circuit model. The fusion, ohmic-heating and radiation powers are shown as a function of time on Fig. B-2. The MHS Case B appears not to be heating as much as the zero-dimensional model predicts, although the diminished temperatures (Fig. B-2) do not significantly effect the integrated power (Fig. B-2). In order to retrieve the Case A conditions, the line density was decreased by $\sim 7\%$ from $3.4(10)^{19} \text{ m}^{-1}$ to $3.30(10)^{19} \text{ m}^{-1}$, in accordance with the predictions of Fig. 10. The Case C curves given on

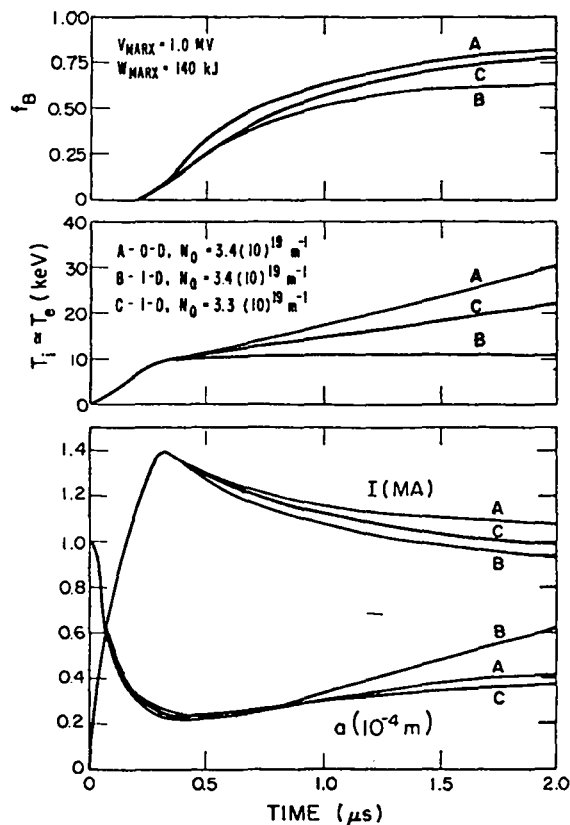


Fig. B-1.

Comparison of zero- and one-dimensional models, showing the time-dependent burnup fraction, temperature, current, and radius.

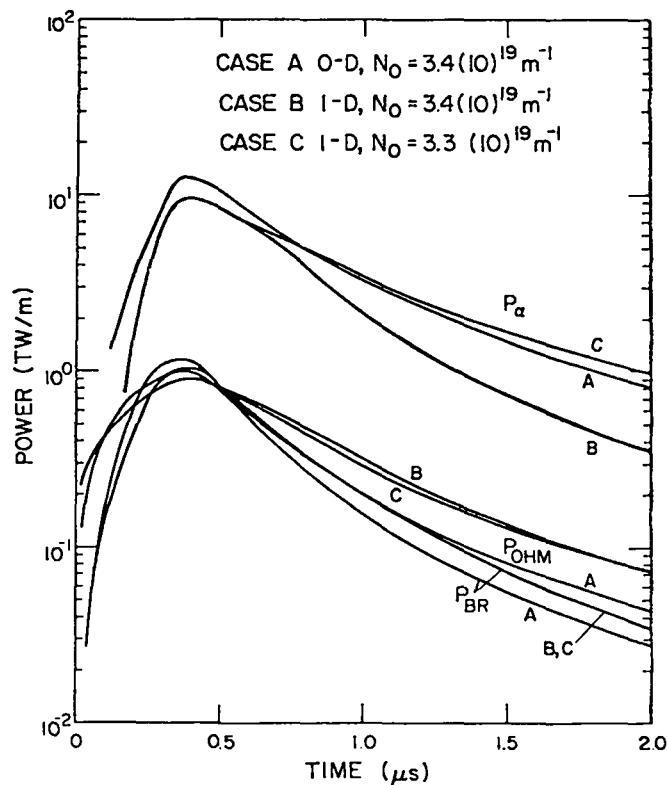


Fig. B-2.

Comparison of zero- and one-dimensional models, showing time dependence of alpha-particle, ohmic and radiation powers.

Figs. B-1 and B-2 depict these results, verifying the extreme sensitivity of the DZP response to line density. Figure B-3 gives the normalized density, temperature, and magnetic field profile at $t = 0$ s (idealized profiles) and $t = 0.5$ s (evolved profiles). Surprisingly little change in radial profiles is predicted by the one-dimensional MHS model. Although the interaction between field transport, plasma compression and mass convection associated with fuel burnup at the center of the DZP is complex, this transport appears to be amazingly rapid in order that the initially-assumed idealized profiles be maintained.

In summary, the agreement between the zero-dimensional and one-dimensional models is surprisingly good, in view of the sensitivity of DZP response to the line density. The small departures from ideal profiles predicted by the MHS model can be explained in terms of:

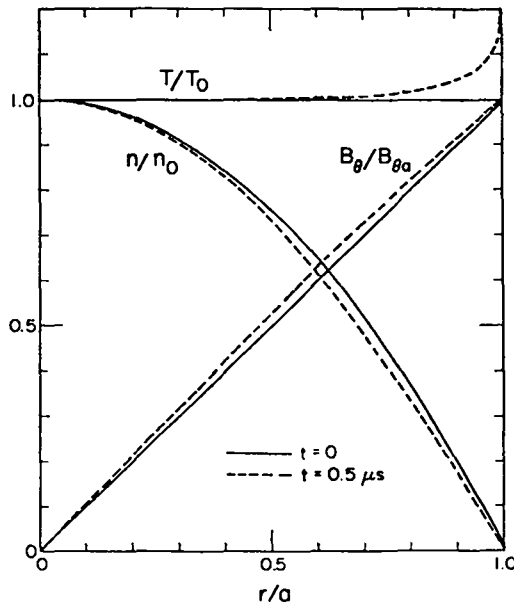
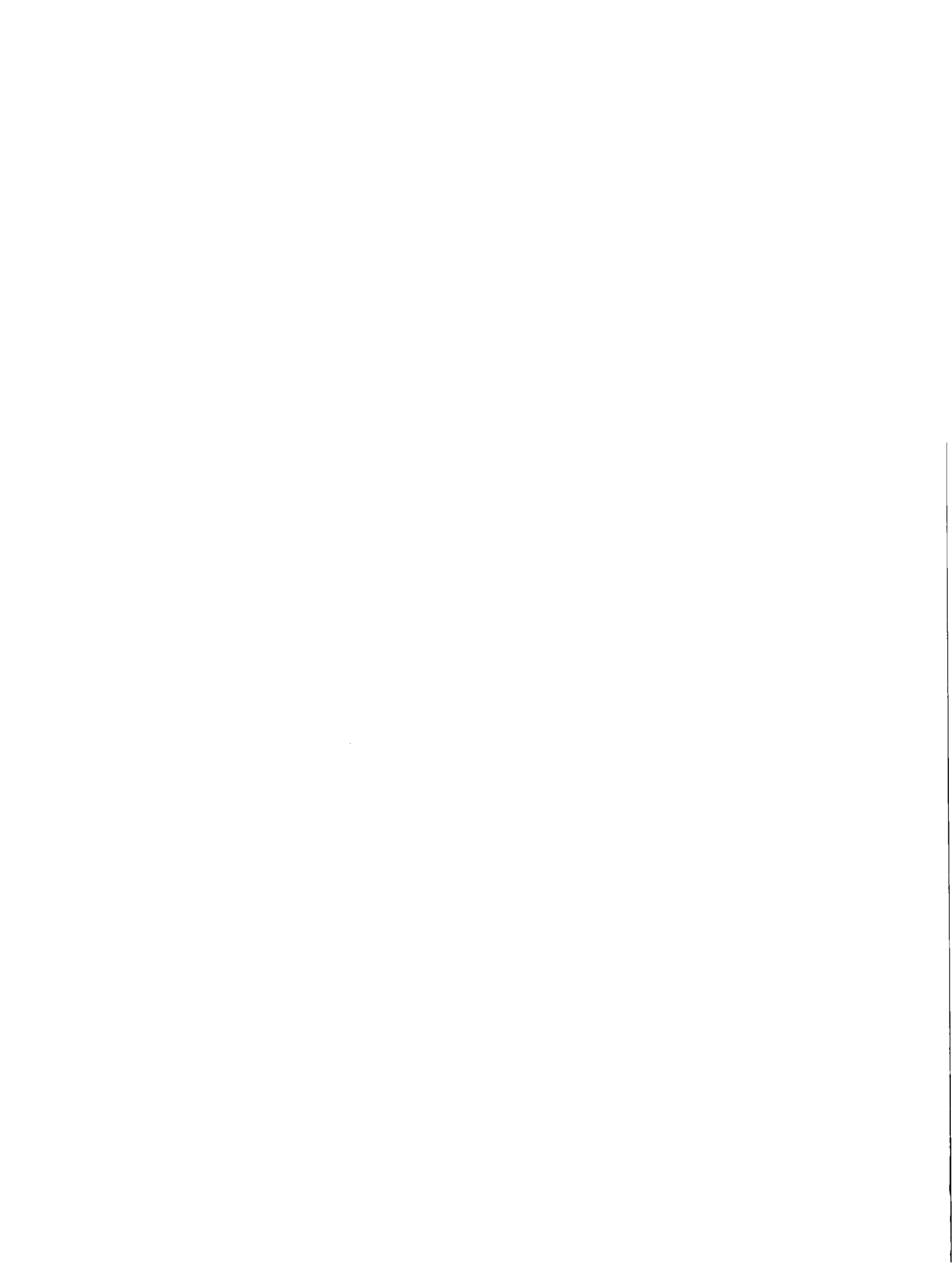


Fig. B-3.

Normalized density, temperature, and field profiles for times during the burn, showing little change in shapes relative to the ideal ($t=0$) shapes.

- Convective effects - Since the heat-capacity ratio, γ , is effectively larger for the plasma under radial compression than for the field, plasma will collect less near the axis, giving less compression near $r = 0$ than at $r \approx a$.
- Transport - The rate of magnetic field penetration into or out of the plasma column depends sensitively on the time-evolving plasma temperature and the field at the plasma surface.
- Fusion Burnup - As plasma is depleted in the center of the column because of the higher fusion reaction rate, field is convected inward, causing departure from the ideal profile.

These processes, when coupled with the highly nonlinear DZP pressure (force) balance, the time-varying plasma current, and the strong spatial variation of radiation losses without alpha-particle heating conspire to present a complex series of interrelated processes embodied in the composite results of Figs. (B-1)-(B-3). Finally, since the plasma center, after the DZP current is established, is heated primarily by radial thermal conduction from the hotter edge region, edge effects that are much more complex than those assumed in these computations will more than likely play an important role in determining the DZP response.



Printed in the United States of America. Available from
National Technical Information Service
U.S. Department of Commerce
5285 Port Royal Road
Springfield, VA 22161

Microfiche \$3.00

001-025	4.00	126-150	7.25	251-275	10.75	376-400	13.00	501-525	15.25
026-050	4.50	151-175	8.00	276-300	11.00	401-425	13.25	526-550	15.50
051-075	5.25	176-200	9.00	301-325	11.75	426-450	14.00	551-575	16.25
076-100	6.00	201-225	9.25	326-350	12.00	451-475	14.50	576-600	16.50
101-125	6.50	226-250	9.50	351-375	12.50	476-500	15.00	601-up	

Note: Add \$2.50 for each additional 100-page increment from 601 pages up.

